Journal of Controlled Release 376 (2024) 1068–1085

Contents lists available at ScienceDirect

Journal of Controlled Release

journal homepage: www.elsevier.com/locate/jconrel

Advancing osteosarcoma 3D modeling *in vitro* for novel tumor microenvironment-targeted therapies development

Sofia Costa [a,b], João Rodrigues [a,b,c], Carolina Vieira [a,e], Sofia Dias [a,b,c], Juliana Viegas [a,b], Flávia Castro [a,b], Bruno Sarmento [a,b,d], Catarina Leite Pereira [a,b,*]

[a] *i3S – Instituto de Investigação e Inovação em Saúde, Universidade do Porto, Rua Alfredo Allen 208, 4200-135 Porto, Portugal*
[b] *INEB – Instituto de Engenharia Biomédica, Universidade do Porto, Rua Alfredo Allen 208, 4200-135 Porto, Portugal*
[c] *ICBAS – Instituto de Ciências Biomédicas Abel Salazar, Universidade do Porto, Rua de Jorge Viterbo Ferreira 228, 4050-313 Porto, Portugal*
[d] *IUCS-CESPU – Instituto Universitário de Ciências da Saúde, Rua Central de Gandra 1317, 4585-116 Gandra, Portugal*
[e] *FMUP - Faculdade de Medicina, Universidade do Porto, Alameda Prof. Hernâni Monteiro, 4200-319 Porto, Portugal*

ARTICLE INFO

Keywords:
Osteosarcoma
Advanced *in vitro* modeling
Immunocompetent model
Tumor-associated macrophages
Immunomodulation
Drug delivery
Tumor microenvironment

ABSTRACT

Osteosarcoma (OS) represents one of the most common primary bone cancers affecting children and young adults. The available treatments have remained unimproved for the past decades, hampered by the poor knowledge of OS etiology/pathophysiology and the lack of innovative, predictive and biologically relevant *in vitro* models, that can recapitulate the 3D OS tumor microenvironment (TME). Here, we report the development and characterization of an innovative 3D model of OS, composed of OS tumor cells, immune cells (macrophages) and mesenchymal stem cells (MSCs), that formed a multicellular tissue spheroid (MCTS). This fully humanized 3D model was shown to accurately mimic the native histological features of OS, while innately leading to the polarization of macrophages towards an M2-like phenotype, highly aggressive and pro-tumor profile. Upon the exposure to immunomodulatory molecules, the MCTS were shown to be responsive by shifting macrophages polarization, and dramatically altering the TME secretome. In agreement, when treated with immunomodulatory/stimulatory nanoparticles (NPSs), we were able to revert the TME secretome towards an anti-inflammatory profile. This study establishes an advanced 3D OS model capable of shedding light on macrophages and MSCs contributions to disease progression, paving the way for the development of innovative therapeutic approaches targeting the OS TME, while providing a biologically relevant *in vitro* tool for the efficacy screening of novel OS therapeutic approaches.

1. Introduction

Osteosarcoma (OS) is the most frequent primary bone cancer [1], affecting mainly children and young adults. This type of tumor is recognized by its high malignancy, due to the local aggressiveness and rapid systemic metastases to the lung [2]. In the past 30 years, available treatments have failed to improve the 5 years-survival rates, of 70–75 % in localized tumor and of 20–30 % in metastatic disease [3]. The persisting ineffectiveness of these treatments is intricately linked to genomic, transcriptomic and epigenetic heterogeneous nature of OS, its resistance to chemotherapy and drug toxicity, and rapid blood clearance, all of which substantially impede positive treatment outcomes [4]. The quest for innovative therapeutic interventions against OS has faced a dual challenge in both scientific and clinical realms for several decades, primarily due to a limited understanding of the pathophysiology of OS and the inadequacy of *in vitro* and *in vivo* models currently in use to study this type of tumor. Recent studies employing 2D/3D *in vitro* models [5,6] and *in vivo* [7,8] preclinical models advanced our understanding of drug resistance mechanisms, tumor progression, and the key events underlying lung metastases. However, these models fall short in replicating the complexity of the OS tumor microenvironment (TME), being unable to fully dissect the existing cell-cell and cell-extracellular matrix (ECM) interactions, as outlined in a recent review of our team [4]. While OS animal models have yielded valuable insights into responses to pharmacological intervention, tumor cell arrest, extravasation, and lung colonization [9], it's important to note that data from animal studies often poorly reflect human disease mechanisms. Furthermore, limited access to clinical OS samples due to the low

* Corresponding author at: i3S – Instituto de Investigação e Inovação em Saúde, Universidade do Porto, Rua Alfredo Allen 208, 4200-135 Porto, Portugal.
E-mail address: catarina.pereira@i3s.up.pt (C. Leite Pereira).

https://doi.org/10.1016/j.jconrel.2024.10.068
Received 13 September 2024; Received in revised form 28 October 2024; Accepted 30 October 2024
Available online 8 November 2024

incidence of the disease and restricted patient material poses a significant challenge. The limitations of existing models emphasize the critical need for innovative approaches that could more accurately recapitulate the TME and the OS pathophysiology. Addressing this gap through the development of a fully human and biologically relevant *in vitro* model is crucial and represents a substantial unmet pre-clinical need in the field. The immune cell population, specifically tumor-associated macrophages (TAMs), has recently emerged as potential targets for OS treatment. The role of TAMs in OS is associated with angiogenesis, increased tumor invasiveness capacity, modulation of TME, and therapeutic resistance [10]. While TAMs infiltration is commonly linked to a poor prognosis in many solid tumors, this association is not consistently observed in OS. Some studies suggest a correlation between TAMs infiltration and metastases inhibition [11], others contend the opposite role [12]. This discrepancy can be attributed to the high functional plasticity that characterizes macrophages phenotypes. The M1 phenotype is associated with anti-tumor effects, whereas the M2 phenotype is described as protumorigenic [13]. In OS, the understanding macrophage polarization impact on tumor progression and therapy. Recent studies indicate the presence of an increased M1 population in non-metastatic OS tumors [14], while inhibiting M2 polarization has been linked to decreased metastasis in OS, emphasizing the potential of immunomodulation as a promising therapeutic approach [15]. Another crucial element in this intricate and highly dynamic environment is the presence of mesenchymal stem cells (MSCs). MSCs role on tumor settlement, progression and metastasis has been recognized. MSCs impact on cancer cells dynamics through the release of growth factors that promote cancer cell proliferation and epithelial-mesenchymal transition (EMT), as well as alter the TME immunocompetence, namely through the recruitment of monocytes and macrophages, fostering drug resistance [16–18].

Bearing in mind the role of each cell population and the ECM of the solid tumor in response to treatment, it becomes evident that preclinical *in vitro* screenings of novel therapies require an adequate model that takes into consideration all these players. Herein, we report a pioneer 3D model of OS, capable of resembling key aspects of the human disease and recapitulating the aggressiveness of this tumor *in vitro*, shedding light on macrophages and MSCs contributions to the OS TME and response to external stimuli, grounding the work for the development and screening of innovative therapies targeting the TME.

2. Materials & methods

2.1. Cell culture conditions

The OS cell line MG63 commercially acquired from ATCC (CRL-1427) (USA) and expanded Dulbecco's Modified Eagle Medium (DMEM, Gibco) with 10 % (*v*/v) heat-inactivated FBS (PAN-Biotech), 100 U/mL penicillin, and 100 mg/mL streptomycin (P06–07100, PAN-Biotech; P/S). Medium was changed every 2–3 days and when ~80 % of confluency was reached, cells were subcultured. Human bone marrow MSCs (hbm-MSCs) were commercially acquired from Innoprot (P10576), expanded and maintained in 1 % gelatine coated flasks with Mesenchymal Stem Cell Medium Kit (MSCM, P60115, Innoprot) with 5 % (*v*/v) FBS, 1 % Mesenchymal Stem Cell Growth Supplement (MSCGS) and 1 % P/S solution. Medium was changed every 2–3 days and cells were subcultured when ~80 % of confluency was reached. Cells were kept in an incubator, at 37 °C, in a humidified atmosphere with 5 % CO_2.

2.2. Monocytes' isolation

Monocytes were isolated from buffy coats of healthy blood donors kindly provided by the immunohemotherapy department of Centro Hospitalar Universitário São João (CHUSJ), Porto, Portugal, under the ethical agreement number: 90/19. Donors provided written consent for their blood to be used for research purposes. For each experiment, blood samples were collected from three different donors and then processed in aseptic conditions. Firstly, samples were centrifuged (1200 rpm, 30 min) and the peripheral blood mononuclear cells (PMBCs) were collected. To isolate monocytes, RosetteSep™ Human Monocyte Enrichment Cocktail (15028, STEMCELL Technologies) reagent was used according to the manufacturer's instructions. Afterwards, the mixture was diluted in PBS + 2 % FBS, added drop by drop in the new tubes containing Histopaque®-1077 (10771, Sigma) and centrifuged for (1200 *g*, 30 min). Monocytes were collected, washed 3× and resuspended in Roswell Park Memorial Institute (RPMI) medium.

2.3. Microtissues formation (mono-, double- and triple-culture)

MicroTissues® 3D Petri Dish® micro-molds were used to cast agarose molds and achieve reproducible spheroids (Z764019-6EA, Merck, Fig. 8A or Z764051-6EA, Merck, Fig. 1b), following the recommendations of the manufacturer. Spheroids were produced by the liquid overlay technique, by transferring the different cell suspensions into the agarose molds (Carlsson & Yuhas, 1984; Napolitano et al., 2007). For OS mono-culture spheroids, using only MG63 cells, the recommended seeding density to achieve MCTS with 400 μM in diameter was used (~8,000 cells per spheroid). Micro-molds were afterwards incubated in a humidified atmosphere with 5 % CO_2 for 30 min to allow for spheroid formation (Fig. 1c) and 0.5–1 mL of medium was added to each well. For double culture spheroids, we have optimized a 1:3 ratio of MG63: Monocytes, maintaining the number of cells per spheroid. To establish the triple culture spheroids, a stromal population of hbm-MSCs was added in ratio of 3:1:3 MSC:MG63:Monocytes, maintaining again the number of cells per spheroid. Medium was changed every 1–2 days and spheroids were incubated in a humidified atmosphere, at 37 °C, with 5 % CO_2.

2.4. Microtissues characterization

2.4.1. Size

Morphology and size progression | Spheroids' morphology was monitored by brightfield microscopy at different time points (day 1, 7, 10 and 14) using ZOE Fluorescent Cell Imager (Bio-Rad Laboratories). Six different spheroids were randomly selected, and the acquired images were used for the size progression analysis. Two diameters of each spheroid were measured using the ImageJ software (Rasband, W.S., ImageJ, U. S. National Institutes of Health, Bethesda, Maryland, USA, https://imagej.nih.gov/ij/, 1997–2018.) and the arithmetic media of these values was calculated.

2.4.2. Metabolic activity

CellTiter-Glo® 3D Cell Viability Assay was used to assess spheroids' viability at different timepoints (day 1, 7, 10 and 14). Three spheroids per replica were collected to a transparent 96-well plate in 100 μL of medium and 100 μL of CellTiter-Glo® 3D Reagent were added to each well. The plate was placed in the orbital shaker (5 min, RT) to induce cell lysis and kept static to stabilize the luminescence signal (25 min, RT). The luminescence was recorded in the Synergy Mx (BioTek).

2.4.3. Histology

Paraffin-embedded samples were sectioned into 3 μm sections (Leica RM2255 microtome) and stained with Hematoxylin and Eosin (H&E). These sections were dewaxed in xylene, rehydrated in graded alcohol series of decreasing concentrations, and washed in distilled water. Afterwards, samples were immersed in Gill's Hematoxylin solution (6765008, Lusoplex) for 3 min, dehydrated by immersing them in a graded alcohol series of increasing concentrations, followed by staining with alcoholic eosin (6766008, Lusoplex) for 1 min. For Safranin O/Fast Green staining, dehydrated sections were incubated in Gill's Hematoxylin (Sigma-Aldrich) for 5 min and washed in distilled water. Afterwards, the samples were immersed in 0.4 % Fast Green (Sigma) solution during 5 min as a counterstain, and washed twice in 1 % acetic acid.

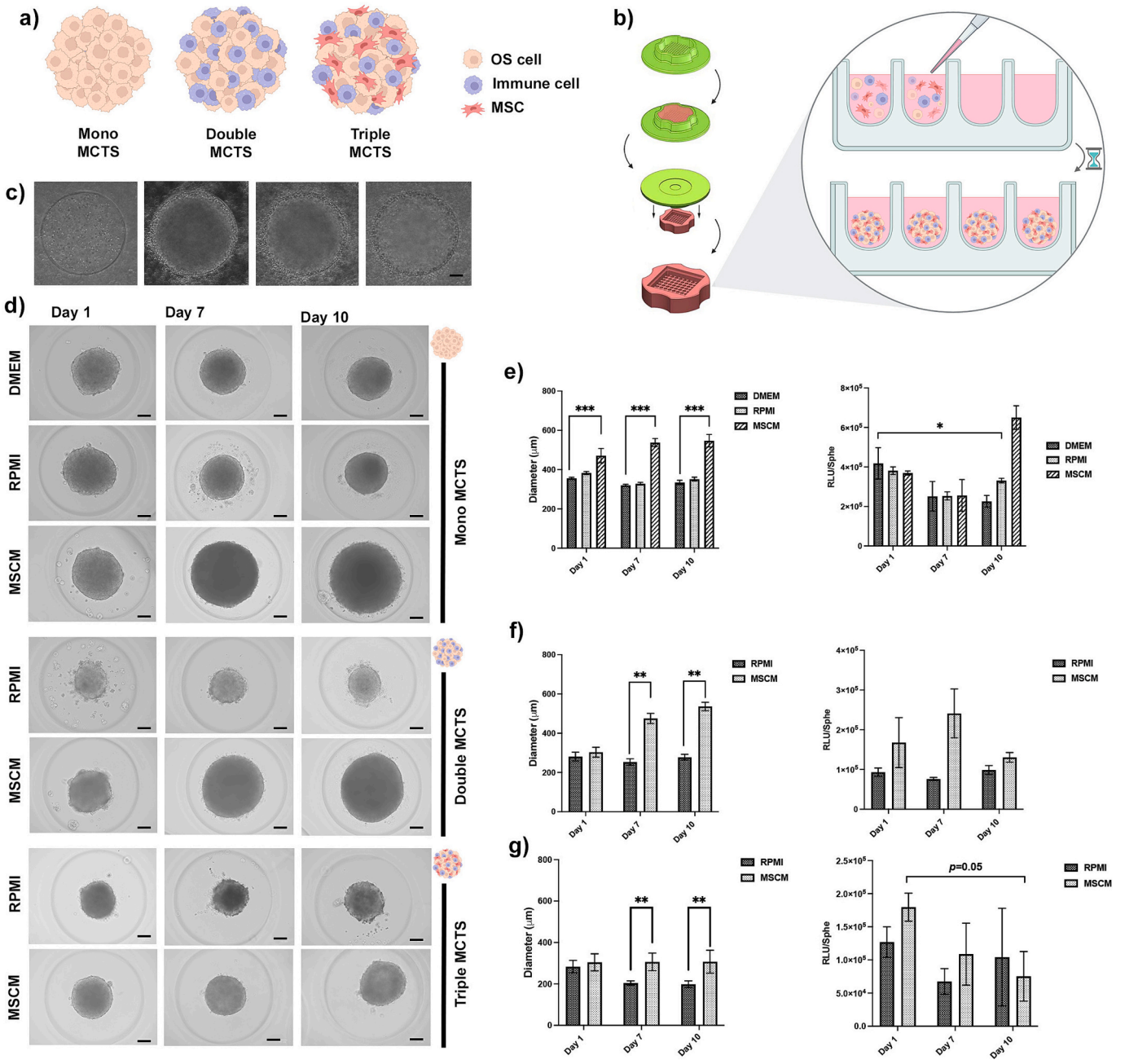

Fig. 1. MCTS formation, size and metabolic activity progression during time. a) Schematic figure of generated mono, double and triple MCTS; b) Protocol for spheroids formation using micromolds; c) Time-lapse images of spheroids formation using micromolds (cells aggregation in the micro-well). d) Microscopy images of generated MCTS during time, using different culture media (Scale bar: 100 μm); Size and metabolic evolution over time in e) mono MCTS, f) double MCTS and g) triple MCTS ($n = 3$, ONE-way Anova, Kruskal-Wallis test, $^{*}p < 0.05$, $^{**}p < 0.01$).

Sections were then immersed for 30 min in 1.5 % Safranin O (Sigma-Aldrich) solution, which stains orange the proteoglycans. In both staining's samples were finally washed in ethanol, immersed in xylene, mounted with Entellan™ mounting medium (107961, Merck). Images were acquired using Zeiss Axioskop 2 microscope and processed with ImageJ software. Representative images of each sample were acquired using the 10× and 40 magnifications.

2.4.4. Ultrastructure analysis

For ultrastructural analysis, spheroids were fixed with 2 % (*v*/v) formaldehyde, 2.5 % (v/v) glutaraldehyde in 0.1 M sodium cacodylate buffer overnight at 4 °C. Then, the fixative was removed and washes were made with 0.1 M sodium cacodylate. The samples were then post-fixed in 2 % (*w*/*v*) osmium tetroxide in 0.1 M sodium cacodylate buffer for 2 h and stained with a 1 % aqueous uranyl acetate solution for 30 min, dehydrated and embedded in Embed-812 resin. Ultra-thin sections (60 nm thick) were sectioned on an RMC Ultramicrotome (PowerTome, USA) using a Diatome diamond knife, picked up on slot grids, and stained with uranyl and lead citrate for 5 min each. The samples were imaged on a JEOL JEM 1400 transmission electron microscope (JEOL, Tokyo, Japan) and the images were digitally recorded using a PHUR-ONA digital camera (Munich, Germany).

2.4.5. Immunofluorescence

Paraffin-embedded samples were sectioned into 6 μm slides, deparaffinized in xylene and rehydrated in a graded alcohol series of

increasing concentrations. Slides were then incubated in sodium citrate buffer (0.01 M, pH 6) (30 min, 96 °C), to allow antigen retrieval. Samples were permeabilized with 0.25 % TritonX-100 (Fisher Scientific) and blocked with 10 % FBS (*v*/v) in PBS 1× (1 h, RT) and incubated with primary antibodies for collagen type I (600–401–103-0.1, Rockland, 1:100) and for fibronectin (F3648, Sigma-Aldrish, 1:200), in a wet chamber, overnight, at 4 °C. Slides were then incubated (1 h, RT) with the secondary antibody Alexa Fluor 488 (Goat anti-rabbit, A11008, Invitrogen, 1:400) in 5 % (*v*/v) FBS in PBST (0.05 % v/v Tween20, Fisher Scientific). Nuclei were stained with 4′,6-diamidino-2-phenylindole (DAPI) (D4592, Sigma-Aldrich, 1 μg/mL) diluted in 5 % (v/v) FBS in PBST.

2.4.6. Flow cytometry

Flow cytometry (FC) was used for cell population characterization and quantification both in double and triple culture spheroids. Briefly, ~40 spheroids per condition were harvested from the micromolds to 15 mL tubes and centrifuged for 5 min, at 1200 rpm, 4 °C, and then washed with PBS 1× by centrifugation. To dissociate the microtissues into single cells, all samples were incubated with 400 μL Versene (15 min, 37 °C), followed by a centrifugation (1500 rpm, 10 min, RT) and incubation with 200 μL Accutase (20 min, 37 °C). After a washing step, samples were incubated in an antibody solution (30 min, 4 °C) followed by incubation with the Fixable Viability Dye eFluor™ 780 (eBioscience™) (30 min, at 4 °C) (Table 1). Cells were fixed with 1 % PFA, filtered and analyzed in the BD FACSCantoTM II flow cytometer (BD Biosciences, USA) within a 72 h period. Cluster of differentiation (CD) 14 positive cells were quantified and considered to represent the total immune population, including both monocytes and macrophages (Ziegler-Heitbrock & Ulevitch, 1993). For the phenotype evaluation, CD163 was chosen for quantifying alternatively activated, or M2-polarized, macrophages (Etzerodt & Moestrup, 2013) while CD86 marker was used to for classically activated, or M1-polarized, macrophages (Dong et al., 2016).

2.5. 3D cellular population distribution during spheroids formation

Triple culture spheroids with fluorescent labelled cells (CellTrace™ Yellow Cell Proliferation Kit (Invitrogen™, C34573; 532/561 nm) and the CellTrace™ Far Red Cell Proliferation Kit (Invitrogen™, C34572; 630/661 nm)) were produced following the manufacturer's protocol (Fig. 6a). MSCs were labelled with the CellTrace™ Yellow Cell Proliferation Kit, so they appear yellow, MG63 cells were stained with the Vybrant™ CFDA SE Cell Tracer Kit, and present a green colour, and monocytes were labelled with the CellTrace™ Far Red Cell Proliferation Kit, therefore presenting a red colour. Briefly, cells were trypsinized, counted and kept in a suspension (1), each cell type was labelled according to the manufacturer's protocol (2) and, subsequently, used to produced spheroids as already described (3). Spheroids' images were acquired 24 h after seeding, in the Opera microscope (4). Before image acquisition, Hoechst 33342 (MedChemExpress, HY-15559) was used to stain the nuclei by incubating spheroids in a concentration of 6,7 μg/mL, for 20 min, and washing with Hank's Balanced Salt Solution (Gibco, 14025100; HBSS). Ultimately, fluorescent labelled cells were used to produced triple spheroids, and images were acquired at the defined timepoints, with the objective of following cell proliferation, possible migration, and overall cell rearrangement within the 3D structure over time.

Table 1
Antibodies used for flow cytometry.

Antibody	Species Source	Reference	Manufacturer	Antibody dilution
Anti-CD14-APC	Mouse	21270146X2	ImmunoTools	1:100
Anti-CD86-FITC	Mouse	21480863X2	ImmunoTools	1:50
Anti-CD163-PE	Mouse	556018	BD Biosciences	1:25
APC-Cy7-Fixable Viability Dye eFluor 780	–	65–0865–14	InvitrogenTM	1:10 000

2.6. External stimulus with an immunomodulatory cocktail

MCTS immunostimulation was performed by the treatment with a cytokines cocktail and characterized by FC. Three different groups were defined: a) the non-stimulated spheroids, simply cultured in cell culture media (RPMI 10 % FBS, 1 %P/S); b) the M1-stimulated spheroids (where RPMI was supplemented with LPS (10 ng/mL) + IFN-γ (50 ng/mL) stimulus for 24 h); and c) M2-stimulated spheroids (where RPMI was supplemented with IL-4 (20 ng/mL) + IL-13 (20 ng/mL) + IL-10 (10 ng/mL). Cytokine cocktail was added to the culture media at day 6 of MCTS culture. Both the MCTS and medium was collected after 24 h after stimulus (day 7) and analyzed for their polarization (using the previous described flow cytometry protocol) and secretome analysis, respectively. Media samples from the different days and conditions were collected, centrifuged and immediately frozen until further analysis. Luminex xMAP technology was used for multiplexed quantification of 48 Human cytokines, chemokines, and growth factors in the MCTS medium. The multiplexing analysis was performed using the Luminex™ 200 system (Luminex, Austin, TX, USA) by Eve Technologies Corp. (Calgary, Alberta). Forty-eight markers were simultaneously measured in the samples using Eve Technologies' Human Cytokine Panel A 48-Plex Discovery Assay® (MilliporeSigma, Burlington, Massachusetts, USA) according to the manufacturer's protocol. The 48-plex consisted of sCD40L, EGF, Eotaxin, FGF-2, FLT-3 Ligand, Fractalkine, G-CSF, GM-CSF, GROα, IFN-α2, IFN-γ, IL-1α, IL-1β, IL-1RA, IL-2, IL-3, IL-4, IL-5, IL-6, IL-7, IL-8, IL-9, IL-10, IL-12(p40), IL-12(p70), IL-13, IL-15, IL-17 A, IL-17E/IL-25, IL-17F, IL-18, IL-22, IL-27, IP-10, MCP-1, MCP-3, M-CSF, MDC, MIG/CXCL9, MIP-1α, MIP-1β, PDGF-AA, PDGF-AB/BB, RANTES, TGFα, TNF-α, TNF-β, and VEGF-A. Assay sensitivities of these markers range from 0.14 to 50.78 pg/mL for the 48-plex. For data analysis, a Heatmap representation was generated using complexHeatmap package in R (v4.1.2). To evaluate the interactive relationships among groups, linear discriminant analysis (LDA) was generated using MASS (v. 73.-58.2) package, and plotted using ggplot2 (v. 3.4.). LDA vectors were scaled for visualization purposes. Over-representation pathway analysis was performed using ClusterProfiler against GeneOntology (GO) (http://www.geneontology.org). For this analysis, cytokines were considered up or down-regulated based on the fold of enrichment of pairwise comparisons between the different conditions. The set of differentially expressed cytokines were then tested for pathway overrepresentation against the whole cytokine pool.

2.7. 3D model response to an immunomodulatory/stimulatory nanosystem

Muramyl dipeptide (MDP) derivatives, particularly mifamurtide (also known as L-MTP-PE), have shown promise in the treatment of OS, being already approved in Europe for the treatment of non-metastatic OS [19]. Herein, MDP was selected as a model, and already approved in clinics, molecule, to validate our OS MCTS responsiveness capacity to currently in use treatment approaches, targeting the TME, particularly immune cells. 3D model response was evaluated using the free molecules and using a Poly Lactic-*co*-Glycolic Acid (PLGA)-based nanosystem, to improve its efficacy. MDP-loaded nanoparticles were produced by water-in-oil-in-water (w/o/w) double emulsion technique. Briefly, the organic phase of MDP-NPs, composed of 20 mg of polymer, Poly Lactic-*co*-Glycolic Acid (PLGA)-COOH (50: 50 LA: GA ratio (PLGA 5004 A, 44 000 Da, PURASORB®, Corbion/Akina, Inc. (PolySciTech)) 50 % (*w*/*v*) was dissolved in dichloromethane (1 mL); the aqueous phase of the MDP-NPs was composed of MDP solubilized in water (2.5 μL of 10 mg/mL MDP stock solution were added to 97.5 μL of MilliQ® ultrapure

water, resulting in an aqueous phase with a MDP concentration of 250 μL/mL). Afterwards, the aqueous phase was added to the polymeric solution and homogenized using a Bioblock Vibracell™ sonicator (Sonics & Materials, Connecticut, USA) for 2 min at 70 % of amplitude, forming the first emulsion (w/o). Further, the w/o emulsion was added to PVA (2 % (*w/v*), 4 mL) aqueous solution and homogenized for 2 min at 70 % amplitude, using the same equipment, forming the second emulsion (w/o/w). The w/o/w emulsion was then poured to PVA (2 % (w/v), 7.5 mL) and left for 2 h under magnetic stirring (300 rpm) to evaporate the organic solvent. After 1.5 h of magnetic stirring, NPs were concentrated by centrifugation using a high-speed centrifuge Beckman Avanti™ J 25 (Marshall Scientific, New Hampshire, USA) at 30,000 g for 20 min at 4 °C, to remove the unloaded MDP and the excess of PVA. Finally, the supernatant was collected, and the NPs pellet was washed once with 10 mL of MilliQ® ultrapure water (30,000 g, 20 min, 4 °C), resuspended in 1 mL of MilliQ® ultrapure water and stored at 4 °C for further experiments. Nanosystems were characterized regarding average size (*Z*-average) and polydispersity index (PdI) by the dynamic light scattering (DLS) method, and zeta-potential (ζ-potential) by electrophoretic light scattering (ELS), using a Malvern Zetasizer Nano ZS instrument (Malvern Panalytical, Malvern, UK). All the samples were dispersed (1:100) in a NaCl (10 mM) solution (1 mL in total). Three measurements were performed for each formulation and four different formulation batches were analyzed (in addition to three empty NP batches). MDP encapsulation efficacy (EE) was determined by an indirect method, through the quantification of the peptide in the supernatant using the Fluorescamine assay. Fluorescamine, used for the detection of primary amines, was purchased from Sigma-Aldrich (Massachusetts, USA). This test was performed by adding of 100 μL of each standard (0 μL/mL to 200 μL/mL of MDP) or sample into the wells of a black 96-well plate, with a clear bottom, already containing 100 μL of MilliQ® ultrapure water. 50 μL of the fluorescamine solution were then added to each well, followed by 15 min at RT incubation in the dark. Consecutively, the fluorescence values were measured in the BioTek Synergy MX microplate reader (BioTek Instruments Inc., Vermont, USA) at excitation and emission wavelengths of 400 nm and 460 nm, respectively. All the samples were measured in triplicates and the fluorescence values were applied to calculate the EE of the formulations. The mean blank's value is subtracted from each sample's fluorescence value and these values are converted to a MDP concentration, based on the fluorescence values of the standard calibration curve. The EE is then calculated as shown in Eq. (1):

$$\text{EE}\ (\%) = \left(1 - \frac{\text{MDP concentration of each sample}}{\text{Total concentration of MDP}}\right) \times 100 \qquad (1)$$

After NPs optimization, Mono, double and triple culture spheroids were produced as previously described and incubated with different concentrations of free and NPs-loaded MDP (0.1, 1, 10 and 20 μg/mL, following concentrations previously tested in *in vitro* settings [20]), at day 5, for 48 h. Cell culture media was afterwards collected and the OS MCTS secretome evaluated by multiplex analysis using Luminex xMAP technology. The multiplexing analysis was performed using the Luminex™ 200 system (Luminex, Austin, TX, USA) by Eve Technologies Corp. (Calgary, Alberta). Fifteen markers were simultaneously measured in the samples using Eve Technologies' Human Focused 15-Plex Discovery Assay® (MilliporeSigma, Burlington, Massachusetts, USA) according to the manufacturer's protocol. The 15-plex consisted of GM-CSF, IFNγ, IL-1β, IL-1Ra, IL-2, IL-4, IL-5, IL-6, IL-8, IL-10, IL-12p40, IL-12p70, IL-13, MCP-1 and TNF-α. Additionally, to evaluate the cytotoxicity of the different treatments, spheroids were collected after the incubation period and cell viability analyzed using a Fixable Viability Dye eFluor™ 780 (eBioscienceTM).

2.8. Statistical analysis

The presented results were always performed in triplicates (using different monocyte donors) and are expressed as mean ± standard deviation. All experiments have. For the analysis of statistical significance, two-way analysis of variance (ANOVA) with Kruskal-Wallis or Mann-Whitney post-hoc test, with the significance level set probabilities of $^{*}p < 0.05$, $^{**}p < 0.01$ and $^{***}p < 0.001$. The statistical analysis of these results was performed using Excel and GraphPad Prism 8.4.3. software.

3. Results

3.1. OS multicellular tissue spheroids (MCTS) can be generated in vitro and maintain their viability up to 10 days in different cell culture conditions

Spheroids represent one of the most versatile, tunable and reproducible 3D *in vitro* models [21]. They mimic the 3D structure of the tumor, while allowing the introduction of the different TME players. These features make it possible to study the multiple cell-cell, cell-ECM interactions while promoting ECM synthesis, now recognized as more than structural support component of the TME, but as an active intervener in tumor progression and metastasis formation. The ease of reproducibility of these models underscores their significant potential as innovative tools for drug screening. Using these models as pre-clinical platforms has proven to be a great advantage in cancer research [21]. As such, the primary aim of this work comprised the establishment and characterization of heterotypic multicellular spheroids of OS that comprised: tumor cells (mono), tumor and immune cells (double), and tumor, immune and MSCs (triple) (Fig. 1a). Spheroids were produced by the liquid overlay technique, which consists of transferring the different cell suspensions into agarose micro-molds with microwells (800 μm diameter) (Fig. 1b). Owning to the inherent non-adhesive and hydrophobic characteristics of agarose, cells in these molds tend to aggregate in a spherical-like configuration (Fig. 1c) and form equal size spheroids [22,23]. Upon the formation of the spheroids, the microtissues were maintained in culture for up to 10 days, and characterized regarding their morphology, size, and metabolic activity at different time-points: day 1, day 7 and day 10 (Fig. 1d-g). Using the different culture media, it was possible to produce heterotypic spheroids of OS, but the analysis of different parameters demonstrated that different culture media culture can impact on the microtissues formation, metabolic activity and their size. In mono OS spheroids (Fig. 1d) formed with MG63 OS cells, compact spheroids were obtained, that maintained their spherical shape and compactness over the time in culture. Regardless of the culture in DMEM or RPMI, the morphology, histological features, size, and metabolic activity was shown to be very similar (Figs. 1d-f and 2). In both media, spheroids presented an average diameter of 345 ± 20 μm during the time in culture, while for those cultured in MSCM, a significant increase in size from day 1 until day 10 (up to 544 ± 29 μm) was observed (Fig. 1d). Spheroids cultured in MSCM media were the only ones presenting an evident necrotic core after 7 days in culture (Fig. 2), while this feature was not present in those cultured in DMEM and RPMI. In both DMEM and RPMI a slight decrease in the metabolic activity was observed during the time in culture, in contrast with those cultured on MSCM, in which the metabolic activity was shown to increase at day 10 accompanying the size increase (Fig. 1e). On the follow-up of these results, both RPMI and MSCM cell culture media were selected to proceed with the establishment of double and triple culture spheroids, and also taking into consideration the sensitive cell culture requirements of both immune cells and MSCs. Double spheroids were produced by combining OS MG63 cells and primary monocytes isolated from buffy coats of healthy blood donors, aiming to include the major immune cellular population described in OS tissue, the macrophages [24]. To form these heterotypic microtissues, a cell ratio of 1:3 MG63:Mon, previously optimized by our team (data not shown) was selected, maintaining the

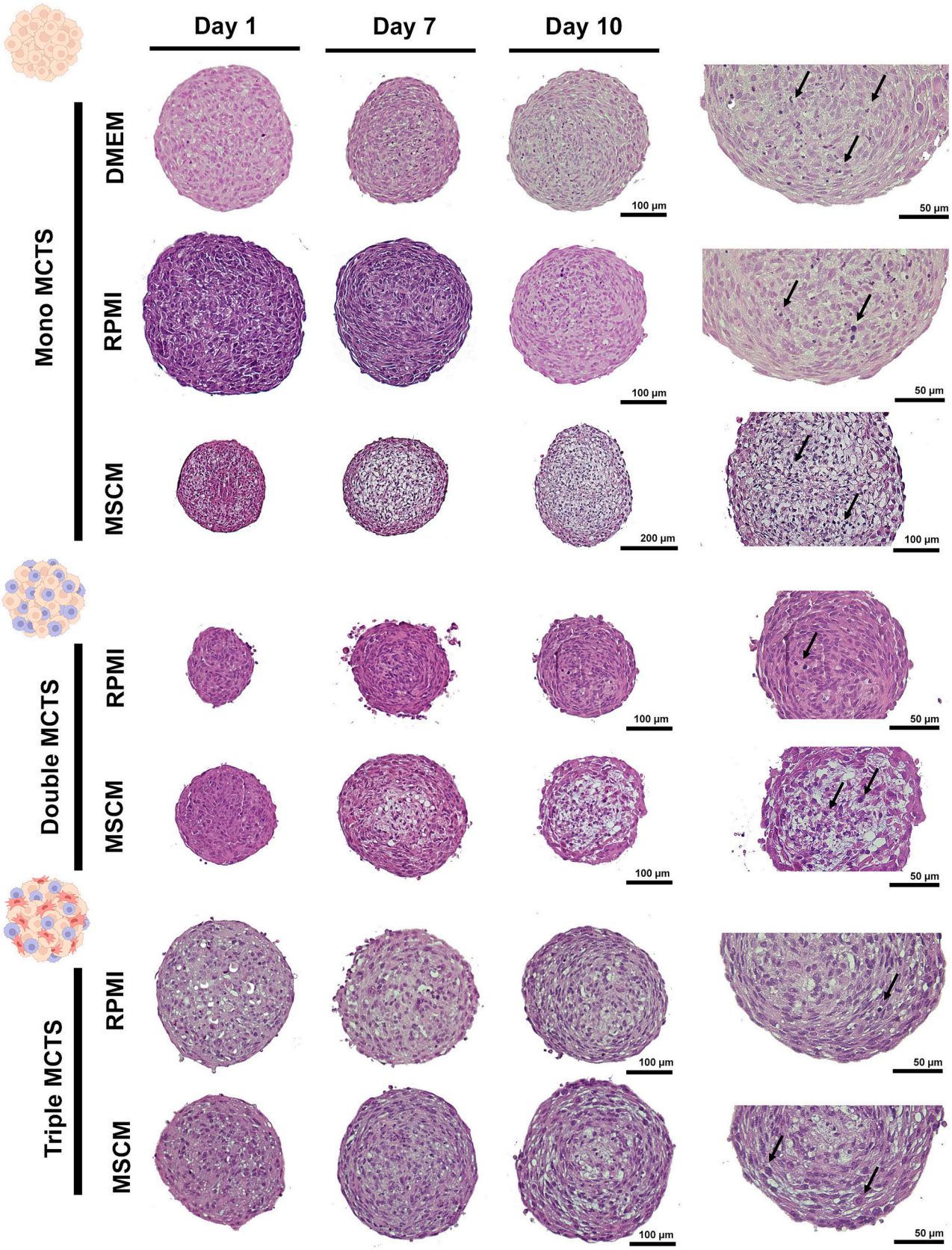

Fig. 2. MCTS organization analysis by histology. a) Representative images of hematoxylin and eosin staining (H&E) staining of generated MCTS over time in different cell culture media (10× magnification). b) Magnification (20×) images of day 10, arrows indicating the pleomorphic and hyperchromatic nuclei in the MCTS. (n = 3).

final cell density per spheroid (8000 cells). Spheroid's formation was achieved using both RPMI or MSCM media, as displayed in Fig. 1d. The addition of immune cells resulted in compact, spherical spheroids, that remained aggregated up to day 10. A significantly smaller diameter of around 277 ± 8 μm was observed in spheroids cultured in RPMI, when compared with those cultured in MSCM (530 ± 6 μm) (Fig. 1f). As for the mono, the presence of a necrotic core was noticed only in MSCM-cultured double spheroids (Fig. 2). These differences in size were not reflected in the metabolic activity values over time, as they were similar up to day 10 (Fig. 1f). The final multicellular 3D model was achieved by adding MSCs to the spheroid composition. MSCs play an important role in the development of OS by modulating the TME and interacting with its different components *via* paracrine communication. They are also known by their immunomodulatory capacities through the secretion of several cytokines and chemokines [25]. For playing such an important role in OS progression, human bone marrow MSCs were chosen to increase the complexity of the multicellular spheroids by introducing a stromal population, highly representative of what is found in an *in vivo* scenario. As for the establishment of mono and double spheroids, also for the triple culture, a density of 8000 cells per spheroid was maintained. MSCs, MG63 cells and monocytes were mixed in a 3:1:3 ratio, taking into consideration that tumor cells have a higher proliferation rate when compared to the other cell types that compose the spheroids [26,27], and previous studies combining MSCs and MG63 [28]. The resultant microtissues were similar in terms of morphology (Fig. 1d), as they presented a spherical shape during the time in culture, with an average diameter of 299 ± 38 μm since day 1 (Fig. 1g). Again, triple spheroids cultured in MSCM exhibited the presence of a small necrotic core, at day 10, could be observed and the size increased progressively overtime, while the metabolic activity decreased. Contrarily, triple spheroids cultured in RPMI, maintained the metabolic activity during the time in culture (Fig. 1g2). Also, the capacity of the MCTS to recapitulate *in vitro* the histological features of the native OS ECM tumor have been studied. For that, all microtissues have been initially stained by H&E (Fig. 2). Regardless of the media used, it was generally observed through this staining that the commonly found in native OS pleomorphic and hyperchromatic nuclei, could also be observed in the MCTS slides (Fig. 2(arrows)).

3.2. Microstructure analysis of the MCTS suggests tumor metabolism alteration in the presence of MSC

Sections of mono, double and triple culture spheroids were analyzed by transmission electron microscopy (TEM) to analyze their ultrastructural. In spheroids composed only of tumor cells (MG63) (Fig. 1S, a (supplementary data)) and in combination with immune cells (Fig. 3a), the common cell ultrastructure could be observed, displaying the organelles seen in eucaryotic cells (nucleus, nucleolus, mitochondria, endoplasmic reticulum, lipid droplet), extracellular vesicles (EVs), the characteristic nuclear polymorphism, and ECM filling the intercellular space. No noticeable differences were observed between these multicellular tissues. However, when analyzing the final model (triple spheroid), with the addition of a stromal cell population (MSCs), a clear alteration of the organelle content was noticed, with an abrupt increase of lipid droplets in the microtissue (Fig. 3b (b5-b8)).

3.3. OS MCTS generated in vitro can emulate the main features of the ECM of the primary tumor

In OS, the ECM undergoes significant alterations that are

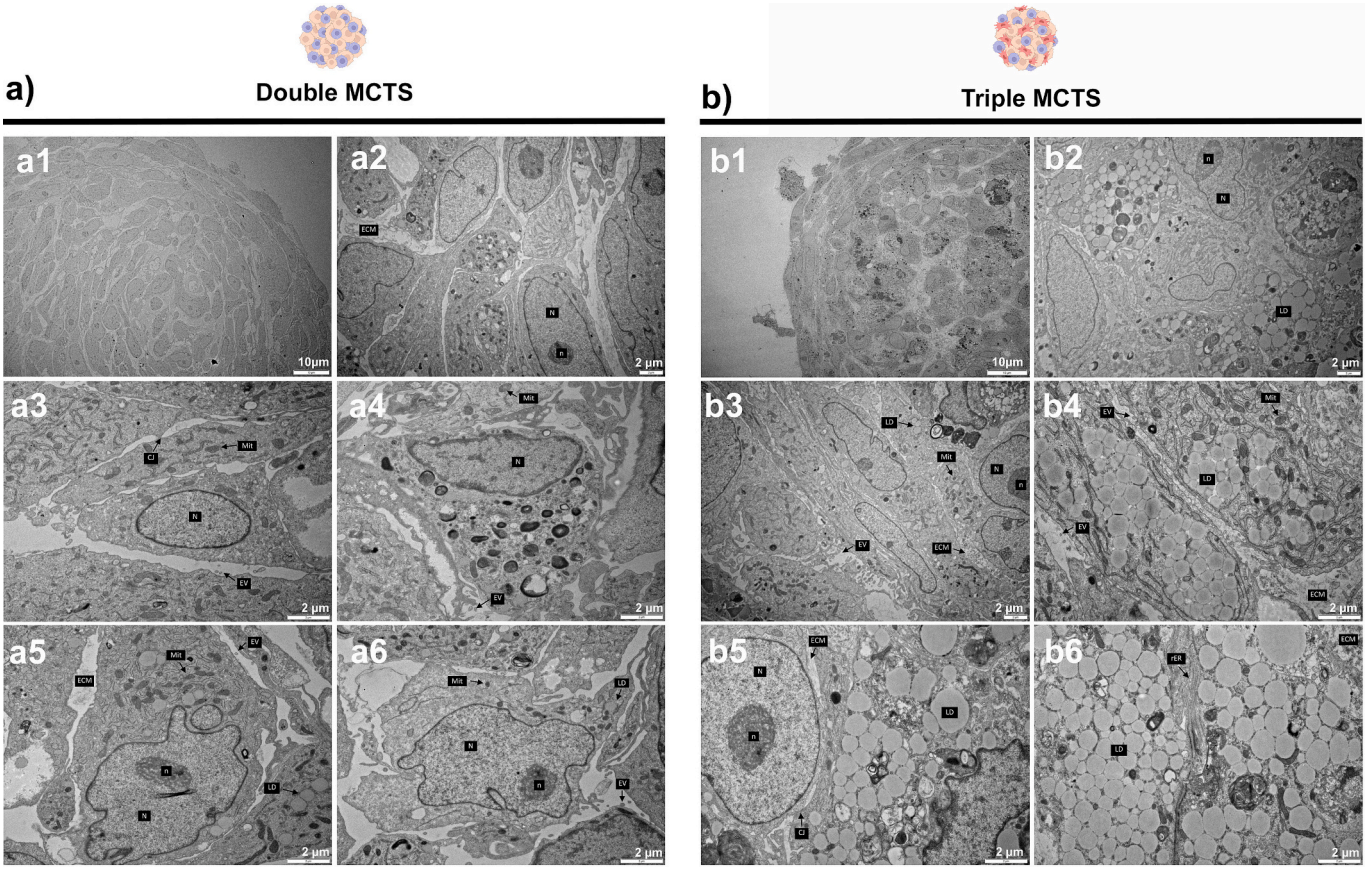

Fig. 3. MCTS microstructure characterization by transmission electron microscopy (TEM). Representative images of the MCTS microstructure of a) double MCTS and c) triple MCTS, images were acquired using 800×, 4000×, 8000× magnification. (Legend: - LD: lipid droplets; N: nuclei; n: nucleolus; rER: rough endoplasmic reticulum; Mit: mitochondria; EV: extracellular vesicle; CJ: cell junction; ECM: extracellular matrix). (n = 3).

characterized by an altered matrix deposition mostly rich in collagen, fibronectin, and other components such as laminin, and proteoglycans contributing to the tensile stiffness and strength, when the tissue is exposed to high strain levels [29]. This ECM is mainly produced by tumor cells, but other stromal cells present in the TME, such as fibroblasts and MSCs, can also contribute to the formation of a dense osteoid matrix [30]. Herein, we have addressed the expression of collagen type I and fibronectin for double and triple spheroids (Fig. 4a and b), while for the final model, we conducted additional characterization, specifically examining the expression of laminin (Fig. 4c) and proteoglycans (Fig. 5) within the tissue. Collagen type I expression pattern was shown to vary over time, transitioning from a widespread expression in the MCTS to a more pronounced expression in the peripheral regions of the tissue (Fig. 4). This pattern was more evident for double spheroids (Fig. 4a3–6), while in triple spheroids, the typical lacy but widespread expression was common to both cell culture medium (RPMI and MSCM) (Fig. 4a7–12). Fibronectin, which is reported to be mostly produced by cancer associated fibroblasts and MSCs [31], has been associated with higher cell migration and tumor aggressiveness. In our MTCS, fibronectin expression was observed in all conditions, with higher intensity in spheroids produced in RPMI media for triple spheroids, and with a slightly different pattern when compared with those cultured in MSCM

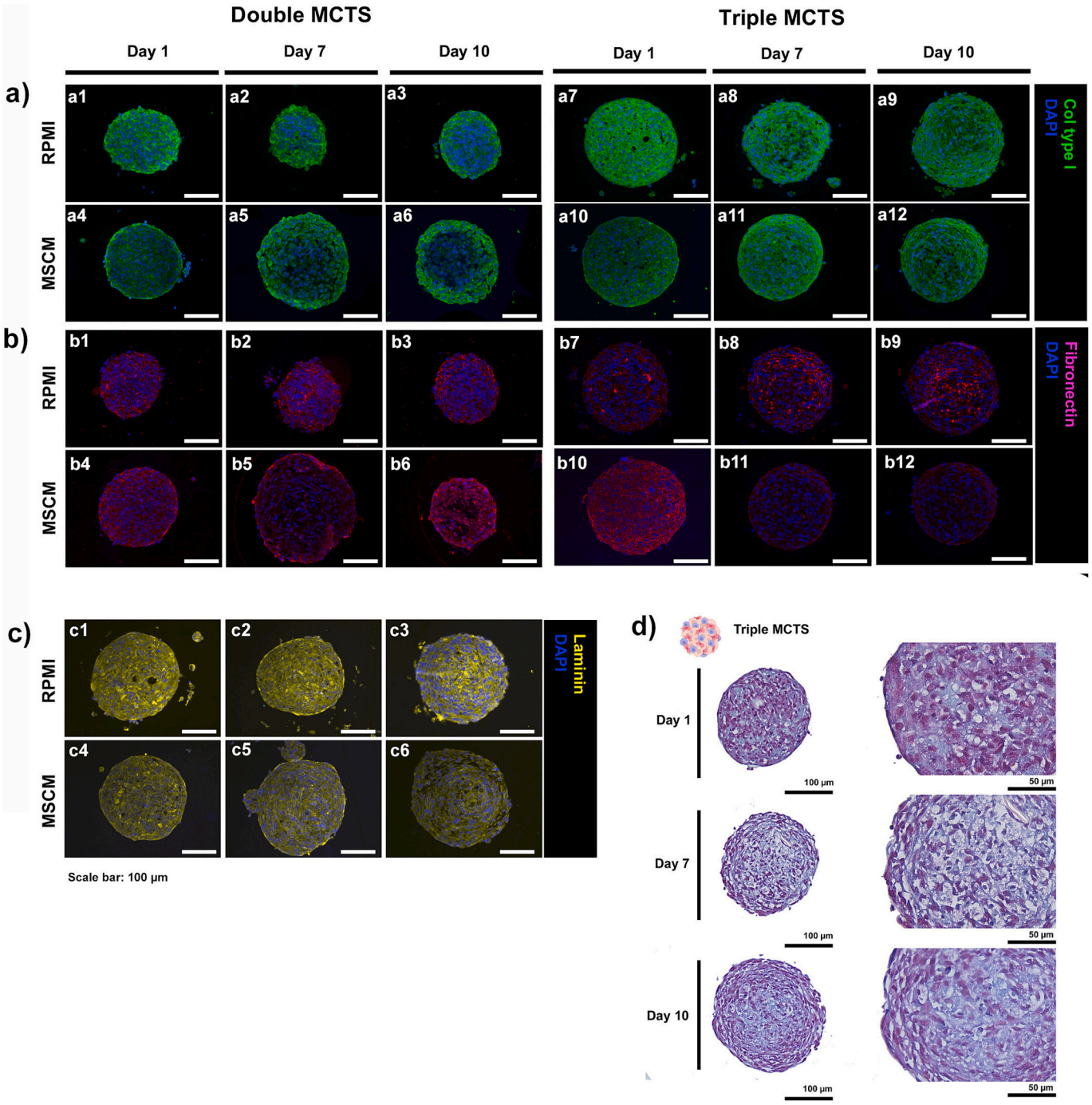

Fig. 4. MCTS ECM analysis by immunofluorescence and Safranin-O green. Representative images of MCTS ECM proteins expression in different media for double and triple cultures: a) Collagen type I, b) fibronectin, c) laminin (n = 3). d) Proteoglycans deposition analysis in the final spheroid (triple culture) (n = 3). (For interpretation of the references to colour in this figure legend, the reader is referred to the web version of this article.)

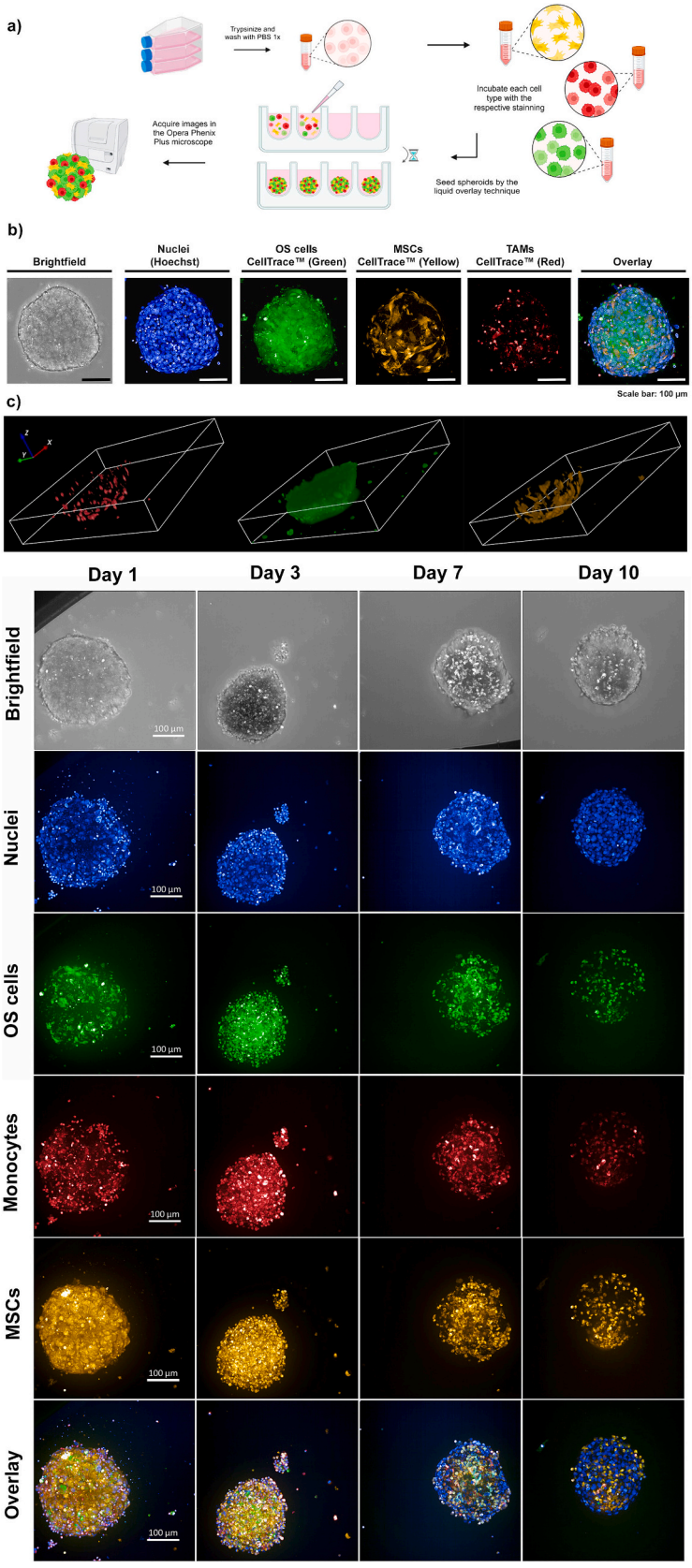

Fig. 5. Three dimensional and spatial distributions of each cell population. a) Protocol of cell labeling for 3D assessment of spatial distribution; b) Cell labelling of each individual cell at day 3 using cell trackers; c) 3D spatial distribution of cell in the triple MCTS; d) Cell populations evolution overtime. (n = 3).

(Fig. 4b). Both double and triple MCTS in MSCM show a peripheric expression of fibronectin, more evident with time (Fig. 4b4–6 and b10-b12), while for triple spheroids in MSCM, fibronectin expression decreases in the tissue (Fig. 4b10-b12). In RPMI, the expression is widely spread and super intense when you have the stromal component of the microtissue, the MSCs (Fig. 4b1-b3 and b7-b9). In the final spheroids, composed of OS, immune and stromal cells, we have further analyzed the expression of laminin. This protein has been associated with angiogenesis, invasion and metastasis, being particularly important in the invasiveness of OS cells [30]. In our study, we have addressed the pattern of laminin expression over time. The results, depicted on Fig. 4c, showed an overall expression identical to fibronectin, being evident that a higher expression was found in the triple spheroids cultured in RPMI (Fig. 4c1-c3), when compared to the MSCM. When observing the Safranin-O-green staining, the osteoid like matrix of the MCTS was even more evident. The typically lacy pattern of immature bone could be noticed in the triple MCTS (Fig. 4d), with the characteristic matrix, rich in proteoglycans (in light blue), whose deposition increases (red/pink staining) with time in culture.

3.4. OS MCTS content and spatial distribution analysis confirms the heterotypic culture of OS MCTS over time and the persistence of both immune cells and stromal cells within the 3D model

The cellular content of the MCTS was analyzed by microscopy, aiming to characterize the final composition of the triple spheroid, and 3D distribution of the different cell populations. To achieve this, the three cell types were stained individually with different dyes and then

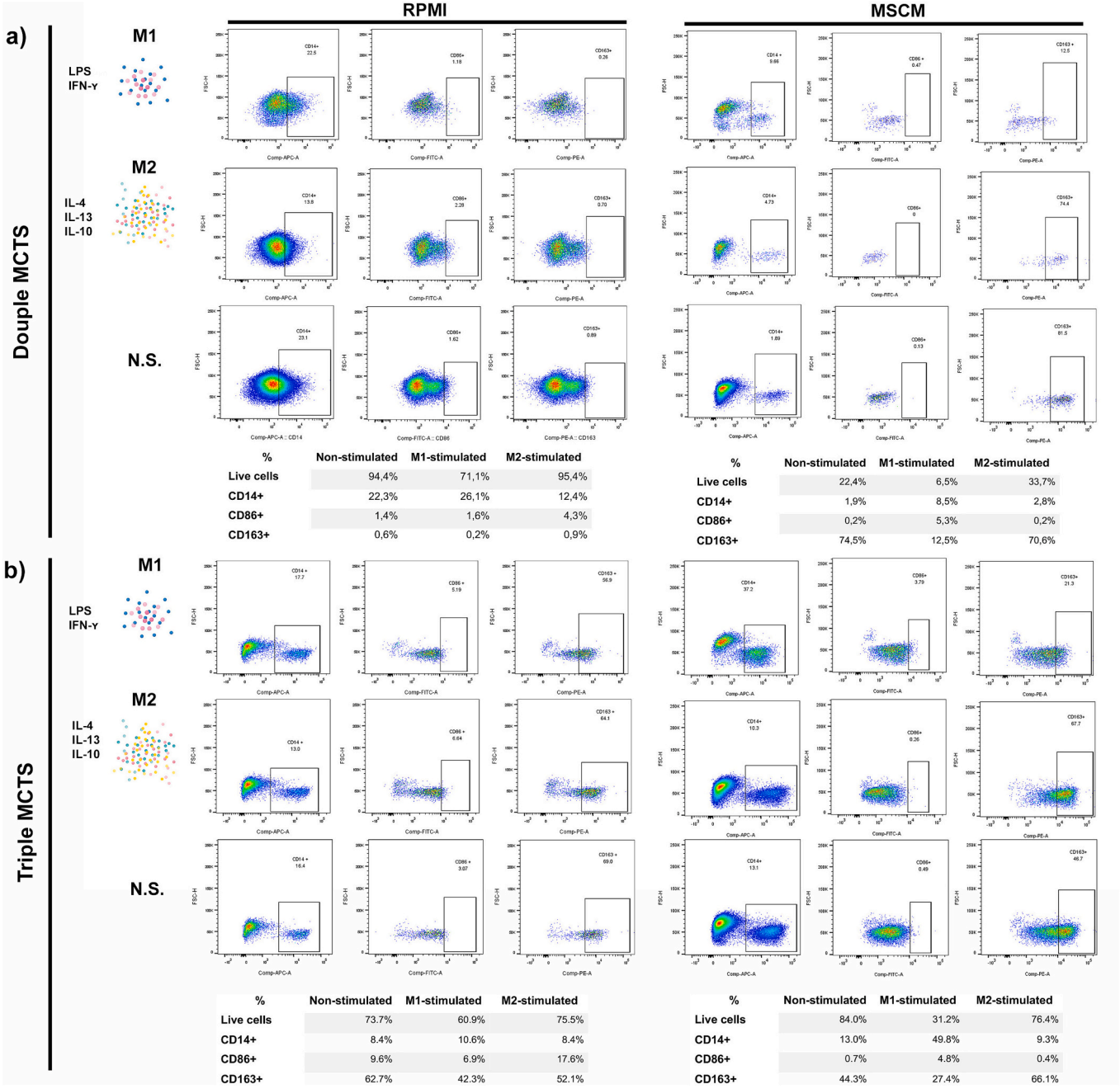

a)

%	Non-stimulated	M1-stimulated	M2-stimulated
Live cells	94,4%	71,1%	95,4%
CD14+	22,3%	26,1%	12,4%
CD86+	1,4%	1,6%	4,3%
CD163+	0,6%	0,2%	0,9%

%	Non-stimulated	M1-stimulated	M2-stimulated
Live cells	22,4%	6,5%	33,7%
CD14+	1,9%	8,5%	2,8%
CD86+	0,2%	5,3%	0,2%
CD163+	74,5%	12,5%	70,6%

b)

%	Non-stimulated	M1-stimulated	M2-stimulated
Live cells	73.7%	60.9%	75.5%
CD14+	8.4%	10.6%	8.4%
CD86+	9.6%	6.9%	17.6%
CD163+	62.7%	42.3%	52.1%

%	Non-stimulated	M1-stimulated	M2-stimulated
Live cells	84.0%	31.2%	76.4%
CD14+	13.0%	49.8%	9.3%
CD86+	0.7%	4.8%	0.4%
CD163+	44.3%	27.4%	66.1%

Fig. 6. Characterization of MCTS immunophenotype by flow cytometry. a) Characterization of double MCTS in RPMI and MSCM. Dot plot of CD14+ cells and subpopulations CD86+ and CD163+ and respective table with quantifications; b) Characterization of triple MCTS in RPMI and MSCM. Dot plot of CD14+ cells and subpopulations CD86+ and CD163+ and respective table with quantifications. (n = 3).

mixed in the appropriate ratio to produce fluorescent triple spheroids (Fig. 5a). Staining of each cellular type with the respective cell tracer was confirmed at day 3, as well as cells spatial distribution in 3D (Fig. 5b-c). Each cell population organization in 3D was afterwards followed-up over time, at day 1, 3, 7 and 10 (Fig. 5d). Our results show that MCTS, as expected, day at day one, the smaller cell population was the OS tumor cells, owning to the used cell ratio of 3:1:3 (MSCs:MG63: Monocytes), but with time that different is dimmed, reaching a point where cells reach the same proportion, demonstrated the good integration in the spheroid, namely of immune and stromal cells, as well as their persistence over the time in culture (Fig. 2S).

3.5. MCTS cell culture conditions impact immune cell population in vitro

Immune cells, namely macrophages that are naturally recruited to the OS TME can either act by fighting the tumor, or further promote OS cells proliferation and consequently favor the tumor progression and invasion [32]. This dual acting capacity is greatly dependent on their polarization in the solid tumor. In highly aggressive OS tumors, most of the reported studies point to an enrichment of M2-like macrophages in the tumor tissue [33–35]. In this study, our objective was also to investigate the polarization of macrophages in the developed OS MCTS, along with assessing the influence of multiple cell populations and the media employed. To this aim, both double and triple MCTS have been cultured in RPMI and MSCM, and the immunophenotype of the macrophages composing the OS MCTS was evaluated by flow cytometry at day 7. Two phenotypic markers within the CD14+ population (monocytes/macrophages), have been used to identify the classically activated/M1-polarized macrophages (CD86), and the alternatively activated/M2 polarized macrophages (CD163). Data has shown that in the case of double spheroids, the use of RPMI medium has favored significantly the immune population, reaching an average population of over 20 %, when compared to the 4.4 % CD14+ cells in the spheroids cultured in MSCM (mean of the CD14+ cells in all groups) (Fig. 6a). Contrary to double culture, in the triple spheroids in RPMI, a lower percentage of CD14+ cells were observed as expected (Fig. 6b). In the triple spheroids, the impact of cell culture medium on immune cells population was not evident and no significant differences were found between the two populations (9,1 % for RPMI and 24 % for MSCM (mean of the CD14+ cells in all groups) (Fig. 6b). It was interesting to observe that having the stromal cell population (MSCs) in the 3D model, led to a clear shift in the immune population towards the M2 phenotype, independently of the cell culture medium used and without the presence of external stimulus. In the triple MCTS, the M2-polatized population of macrophages represented around 50 % of the CD14+ population (62,7 % and 44,3 %, in RPMI and MSCM, respectively), while only a small fraction of the CD14+ displayed the CD86+ marker for the M1 phenotype (9,6 % and 0,7 %, in RPMI and MSCM, respectively). These results suggest that the MCTS can innately develop a more aggressive M2-like phenotype only through the addition of a third cell type, the stromal component. This result corroborates what has been described regarding the role of MSCs in modulating macrophage plasticity through multiple microenvironmental signals [36]. High levels of GM-CSF, IL-10, IL-6, and TNF-α secreted by MSCs have been described to trigger an M2-like phenotype in solid tumors [36,37]. In fact, we could observe values of multiple cytokines, as IL-6, IL-10, TNF-α, and chemokines at the initial days of co-culture (day 1 and day 3) in the final OS model (Fig. S3), and that decrease overtime in the majority of donors (of macrophages).

3.6. Triple OS MCTS are responsive to immunomodulatory cocktail stimuli by altering the TME secretome

The TME can be modulated by targeting its immune component, known for their phenotypic plasticity reactive to multiple signals. In our study, we have been able to demonstrate that the developed MCTS displayed a highly aggressive phenotype, being composed of an immune cell population essentially polarized to a M2-like phenotype, in addition to all the ECM indicators. Aiming to addressing the responsiveness of the MCTS to an external immunomodulatory stimulus, that could modulate the tumor TME, triple MCTS were treated with well described M1 and M2 stimulus. For the M1 phenotype, MCTS were exposed to LPS (10 ng/mL) and IFN-γ (50 ng/mL), while for M2 phenotype IL-13 (20 ng/mL), IL-4 (20 ng/mL) and IL-10 (10 ng/mL) were used. In our flow cytometry data, it appears that once established, the macrophages M2-like phenotype resulting from the triple spheroids' TME cannot be overcome by the administered external M1 stimulus (in the tested dose) (Fig. 6). CD86+ population remained low when compared to the CD163+, only slightly increasing in the case of both double and triple spheroids cultured in MSCM (Fig. 6a-b). It is well recognized that TAMs are extremely plastic, heterogenous, and that its polarization is a continuum [38] that might not be clearly reflected in the changes in cell markers, but can impact on the tumors TME, altering the secretome that will ultimately influence cells behavior in the tumor. To verify our hypothesis, we have further evaluated the secretome of non-stimulated, and M1/M2-stimulated triple MCTS using a multiplex assay. The resulting differentially expressed cytokines were illustrated by heatmaps (three replicates (corresponding to each monocytes donor) per group). As anticipated, although a clear polarization of the macrophages was not observed by flow cytometry, a clear shift in the secretome profile was found in the M1-stimulated condition (Fig. 7a). A significant increase of multiple factors with an important role in solid tumors have been identified following the M1 stimuli, as the case of TNF-α (Tumor Necrosis Factor-alpha), MIP-1α (Macrophage Inflammatory Protein-1alpha), RANTES/CCL5 (Regulated on Activation, Normal T Cell Expressed and Secreted), MIP (Macrophage Inflammatory Protein), M-CSF (Macrophage Colony-Stimulating Factor), G-CSF (Granulocyte Colony-Stimulating Factor), FLT3L (FMS-Like Tyrosine Kinase 3 Ligand), IFN-γ (Interferon-gamma), IL-1β (Interleukin-1beta), IL-12p40 (Interleukin-12 subunit p40), IL-15 (Interleukin-15), IL-27 (Interleukin-27), MCP-3 (Monocyte Chemoattractant Protein-3), TGF-α (Transforming Growth Factor-alpha), TNF-β (Tumor Necrosis Factor-beta), IL-6 (Interleukin-6), IL-8 (Interleukin-8), which levels were significantly higher when compared to M2-stimulated group and N.S. (Fig. 8a). In the case of M2-stimulated group, the profile was more similar to the non-stimulated (N.S.) group, although the stimulus has also prompted the significant increase of eotaxin, and Interleukins IL-2/-4 / -10 and − 13 levels (Fig. 8a). Also, it was possible to clearly recognized the three different groups based on cytokine patterns (Fig. 8b). To further elucidate the biological processes involved in the profile changes in cytokines, between the M1- and M2-stimulated groups, we have identified GO (gene ontology) terms in the different groups. Only using differently expressed cytokines ($p < 0.05$) to disclose the enriched categories of biological processes. In brief, in the M1-stimulated group, biological processed linked to the regulation of immunoglobulin production, regulation of b-cell proliferation and activation, immunoglobulin production and B cell proliferation, have emerged (Fig. 8c).

3.7. Nanosystems containing an immunomodulatory compound can modulate OS TME towards an anti-tumoral profile

Nanosystems for drug delivery have been extensively studied in the biomedical field as they carry the promise of overcoming the setbacks seen in conventional treatments, such as off-target toxicity, rapid blood clearance and unfavorable bioavailability. Here, we report the development of polymeric NPs encapsulated with MDP as model and currently in use immunotherapeutic strategy targeting the OS TME, as a way to validate our model responsiveness and its potential in the screening of immunomodulatory therapeutic approaches and other novel drugs for OS. To that purpose, we have first optimized the preparation of the MDP-loaded NPs, that resulted in PLGA-based NPs with an

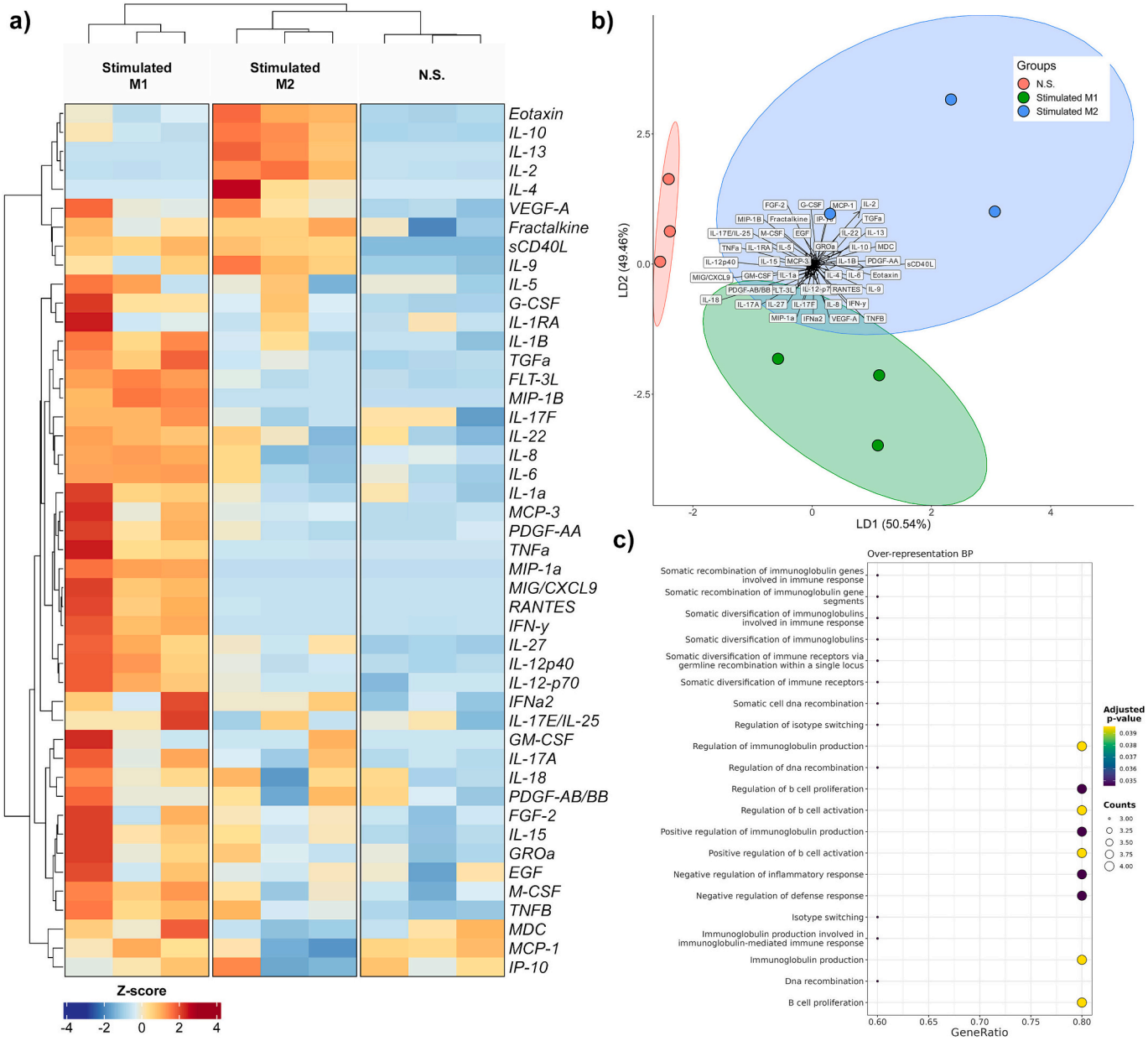

Fig. 7. Triple MCTS secretome analysis after stimulus. a) Heatmap and hierarchical clustering of the different cytokines; b) LDA analysis identifying the cytokines/chemokines that define each examined group. c) GO biological processes enriched among the proteins differently expressed in M1 *vs* M2 group. The X-axis shows the gene ratio, which is the ratio of the specific cytokine numbers to all numbers annotated in the GO pathway. The Y-axis shows the top differently expressed GO pathways with $p < 0.05$. (n = 3).

average size of 197±6 nm and encapsulation efficiency (EE%) of 69± 42 (Table 1S), that were afterwards tested in the triple OS MCTS. First, we evaluated free MDP and MDP-loaded NPs' cytotoxicity in our final model and in the mono spheroids, to rule out any possible toxicity of the particles against tumor cells. Cell viability after exposure to each of the treatments showed no significant decrease in cell viability for all concentrations tested, either in the free or in the encapsulated form of the molecule (Fig. 4S) for triple OS MCTS, while a dose dependent toxicity was observed for mono MCTS. To verify the immunomodulatory and immunostimulatory potential of the NPs in our model, cell culture media was collected from all conditions 48 h after treatment, and the levels of a selected cytokines/growth factors, shown to be secreted by the OS MCTS. We have evaluated how the MDP-loaded NPs impacted the OS TME, namely by modulating its secretome. As controls, we have kept the untreated tumors and both M1/M2 polarized conditions. Multiplex analysis evidenced that the two highest NPs' concentrations (10 μg/mL and 20 μg/mL) were capable of inducing the secretion of soluble factors that resemble the M1-like profile (Fig. 8). For instance, these were the only conditions where we could observe an increase in the TNF-α, IL-1β and IL-6 concentrations, for all donors. Even though our nanosystem was able to induce the production of these M1 signature soluble factors, this was not the case for IL-12p40, IL-12p70 and IFN-γ, which were upregulated exclusively in the M1-stimulated control. Interestingly, free MDP at the same concentrations exhibited limited capacity of modulating the OS TME towards an M1-like profile, highlighting the advantage of using nanosystems for enhanced treatment efficacy. Both free MDP and NPs, at 10 μg/mL and 20 μg/mL, were able to upregulate IL-8 to similar levels as seen in the M1 control, however, free MDP failed to upregulate others.

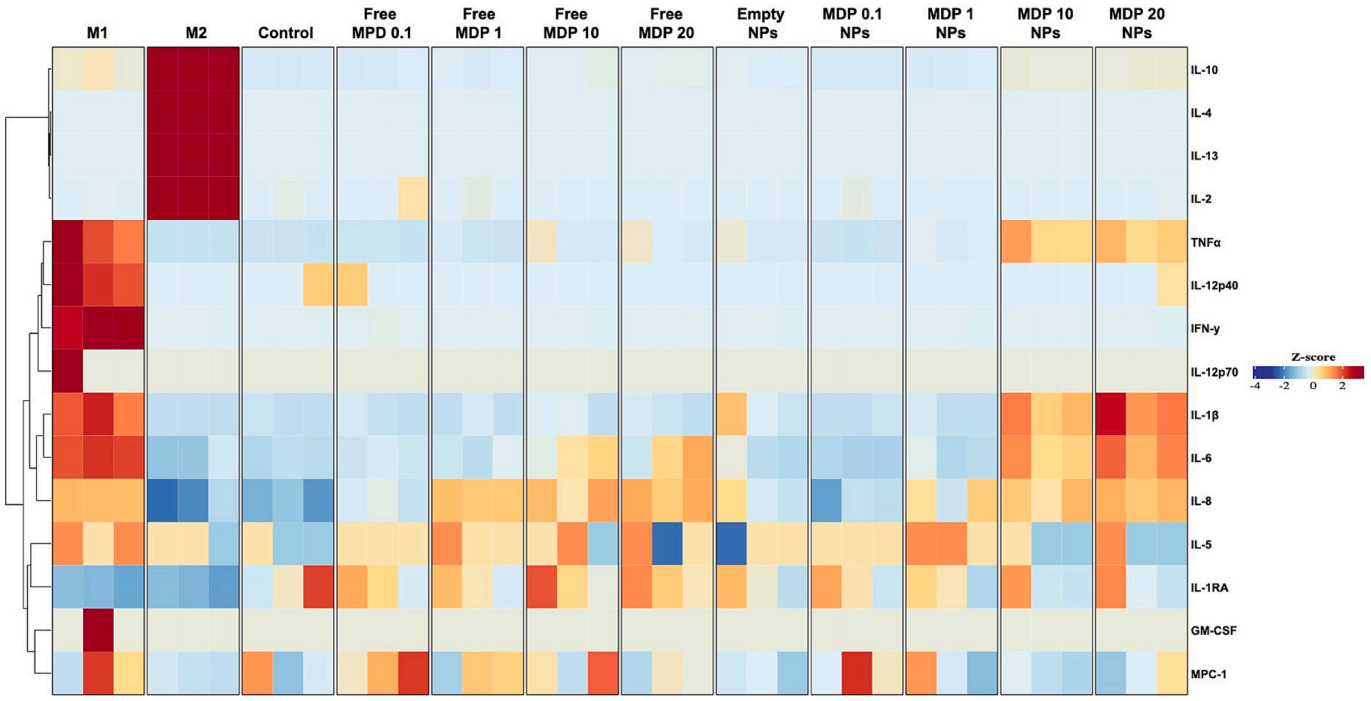

Fig. 8. OS MCTS triple model responsiveness to MDP-loaded NPs. Heatmap and hierarchical clustering of the different cytokines in response to the free and MDP-loaded treatments at 48 h (n = 3).

4. Discussion

In recent decades, there has been a transformative shift in experimental research, moving away from simplistic 2D models and overly complex animal models towards more physiologically relevant 3D *in vitro* systems. This transition is particularly crucial in cancer research, where the limitations of 2D cell models have become evident. Despite their low cost, high reproducibility, and ease of implementation, 2D models fall short in recapitulating key aspects observed in solid tumors, specifically the failure to reproduce crucial cell-cell and cell-ECM interactions in 3D environments [39]. In the context of OS, direct contact with 2D or 3D collagen-based structures results in distinct protein expression profiles in cancer cells, underscoring the importance of a 3D structure in mimicking solid tumors [40]. The inadequacy of 2D models to fully represent the 3D TME has led to the failure of promising drugs at later stages of development, prompting a growing interest in 3D models for drug testing. While there have been significant advancements in exploring 3D models for various cancer types, research on OS lags behind, with much of the knowledge derived from 2D cultures or *in vivo* experiments [4]. This raises concerns about the translatability of the data to humans. Moreover, emerging 3D models often exclusively cultivate tumors cells, even though it is widely acknowledged that models focusing solely on cancer cells fail to capture the intricate network of interactions present in the TME. Few reports have described OS cells co-culture with other TME relevant cell types [41–44], however, as of our current knowledge a heterotypic biomimetic 3D model of OS gathering human cancer cells, monocytes and MSCs, has never been described.

Going beyond the current state of the art, our study established a 3D model of OS, capable of recapitulating *in vitro* multiple features of this solid tumor, offering a novel tool to investigate the progression of the disease, cell-cell interactions and screen novel therapeutic approaches. Culture conditions can significantly impact spheroids features and although such comparison has never been performed for OS spheroids, others studies addressed culture conditions impact on MCTS circularity, compactness [45], as well as cell proliferation and paracrine secretion [46,47], and can critically affect the growth, and proteins secretion implicated in angiogenesis and immune cell interaction, in breast cancer spheroids [48]. In our study, we have shown that for OS, different culture media can impact the formation (size and metabolic activity) and some of the properties of the MCTS (ECM expression patterns), resulting in favorable or not, conditions to all cell types constituting the spheroids. Herein, MSCM contributed to produce bigger spheroids that presented high expression of collagen type-I in the proliferative area (outer area of the spheroid), which might significantly limit nutrient transport and O_2 in the 3D structure, thus inducing a faster necrotic core formation. Although direct comparisons with other studies are challenging due to the unique focus on the media impact on OS spheroids, this study suggests that MSCM promotes the growth of stromal cells, contributing to the formation of larger spheroids with higher collagen type-I expression in the proliferative outer regions. This structural characteristic may impact nutrient and oxygen transport within the 3D spheroid, potentially accelerating the formation of a necrotic core. Notably, Monteiro et al. [43] observed necrotic core development only after 14 days in monoculture spheroids of the MG63 cell line, suggesting that more time of culture would be needed to observe such feature in other conditions. Herein, we also observed a decrease in fibronectin expression under MSCM culture conditions that might reflect the development of a hypoxic core, aligning with prior findings that hypoxia reduces the expression of proteins linked to cellular spread, such as fibronectin [49]. RPMI led to the production of smaller spheroids and was selected has the preferential media for the culture of the triple OS spheroids, maintaining an adequate cellular content (higher amount of CD14+ cells) and ECM expression. Still, of most importance seems to be the cellular composition of the spheroid. TAMs are known for controlling a wide set of disease-related processes, including angiogenesis and the migration of tumor cells [50]. These are also the most abundant immune cell type found in the OS TME [51]. The polarization of TAMs towards the M2 phenotype is associated with a pro-tumoral microenvironment, so the blocking or reversion of this phenotype has been seen has a potential therapeutic approach. This phenotype redirection was already achieved for OS, both *in vitro* and *in vivo*, and proved to be a successful strategy for inhibiting metastases [15]. On the other hand, the role of MSCs in OS progression has been a topic of interest as well. First, it is believed that

OS cells derive from pre-osteoblast MSCs which highlights the importance of the stromal population found in the TME [52]. It is also established that the intense crosstalk between MSCs and OS cells by EVs' secretion is actively involved in the tumor progression and premetastatic niche formation [53]. The pro-tumoral action of these cells and their role in the metastatic process was reported by Xu et al. [54], however, some studies consider MSCs as "double-edged swords", due to their anti-tumoral capacity evidenced in some reports [55]. In our study, ratios of each cell type were optimized accordingly to the proliferating rates of each cell and considering that monocytes differentiation into macrophages will limit this population growth. A ratio of 3:1:3 MSCs:MG63: Monocytes was defined for the final triple culture model based on the doubling time of bone marrow derived humans MSCs (>90 h [27]) when comparing to tumor cells, particularly MG63, that have been reported a doubling time of ~ 48 h [26], but also based on previous studies where MG63 and MSCs have been combined to form OS spheroids at this same ratio, aiming representing an early stage tumor composition [28]. Using this ratio of the three types of cells and the defined culture conditions, we were able to replicate *in vitro* the aggressiveness of OS, as this model was shown to innately polarized towards the M2 immunophenotype, suggesting the TME as the major contributor to the pro-tumoral phenotype of the generated model. Overall, the immune population comprised around 10–20 % of the spheroid total cell population, in line with the values found in the native OS tissue [24]. This could be explained by the presence of a stromal population in the microtissue, known to modulate the TME [56], namely through the secretion, by MSCs, of immunomodulating soluble factors as IL-6, that induce M2 polarization [57]. Also, our data corroborates Tran, et al. studies that demonstrated that by adding a stromal population to breast cancer MCTSs enhanced M2-polarization in THP1-derived macrophages [58].

One of the OS hallmarks is the production of a rich osteoid ECM, that goes beyond simple physiological growth support, modulating the TME and interfering in cell communication [59]. Collagens represent the most prevalent organic constituents of the OS ECM, with collagen type I metabolites shown to be elevated in the serum of OS patients [60]. Fibronectin, an adhesive glycoprotein, is capable of forming a multidimensional fibrillar matrix, significantly contributing to cell adhesion, migration, and differentiation. Its abundance in OS is associated with a poor prognosis, and an upregulation of fibronectin has been observed in chemoresistant OS cell lines [61]. Laminin, linked to angiogenesis, invasion, and metastasis, is particularly crucial in the invasiveness of OS cells [30]. The expression of these ECM components in the developed 3D OS MCTS demonstrates their ability to naturally generate a matrix in culture, mimicking the ECM composition of native tissue. Others have also reported that spheroids derived from various OS cell lines, including MG63, express fibronectin, collagen type-I, and –III [62]. This study also indicated that the addition of stromal cells to OS spheroids increases the expression of ECM proteins. Furthermore, the presence of these ECM components, specifically fibronectin and laminin, in the tissue further supports the aggressive nature of the generated model. Through the interaction of the three cellular components herein combined, the created TME is particularly conducive to tumor development.

An important finding from the ultrastructure analysis of the MCTS was the abundant presence of lipid droplets (LDs) in the final model (triple MCTS) when compared to the mono and double spheroids. These cytoplasmic organelles and endoplasmic reticulum (ER)-derived structures play a pivotal role in energy metabolism, inflammation and signaling, and were found to accumulate in several cancer cell types. In fact, it is now known that LDs are present in all steps of cancer development and act as modulators of the tumor microenvironment [63]. The great increase observed in the triple MCTS suggest an altered metabolic activity, known to be common in cancer cells to support their high proliferation rates, particularly in aggressive cancer types [64]. Interestingly, recent studies in colon cancer suggested that the immunosuppressive of TAMs is regulated by lipid metabolism, particularly unsaturated fatty acids, and LDs proved to be efficient targets for blocking polarization of TAMs *in vitro*, but also for inhibiting tumor growth *in vivo* [65]. High LD content has been described in the past, in OS canine samples, still, it was only possible to recapitulate *in vitro* when using an heterotypic OS 3D model [66]. In human OS, a great increase in LD accumulation was only seen in MCTS submitted to acidosis to support cell survival, and when targeting sphingolipid metabolism *in vivo*, a decrease in the lipid content was accompanied by imbibition of tumor growth [67]. The presence of a higher number of LDs in the final triple model, which was not seen in mono and double MCTS, suggests that an intricated cross-talk between tumor, immune and MSCs was established, representing more accurately the complex OS TME. This also highlights the potential of the our TME representative model as a suitable platform for unravelling the not yet fully understood role of LDs in aggressive cancers and its potential therapeutical value, since some questions regarding LD function in cancer are still unanswered [68].

To address whether we could modulate the immunophenotype of the tumor, and if the developed MCTS were responsive to an external stimulus, immune cells polarization as well as the secretome of the microtissues was evaluated after stimuli with previously described immunomodulatory cocktails [69,70]. Our data has shown a clear shift in the secretome of the triple MCTS when treated with the M1 stimulus, with an increased secretion of multiple cytokines/chemokines know to play a role in both anti-tumor activities, but also in OS progression. MIP-1α [71] has been described to be increased in OS cells lines flowing an M1 stimulus, and namely in the presence of TNF-α, also increased in the M1-stimulated group in our study. RANTES/CCL5, also increased in the M1-stimulated group, has been described to have a role in OS progression by favoring OS cells motility and consequent invasion [72–74], however, CCL5 is a double-edged sword in cancer, has been described to also promotes antitumor immunity by recruiting anti-tumor T cells and dendritic cells to the TME, thus enhancing immunotherapy response in different tumor types [75]. IFN-γ plays a key role in activation of cellular immunity and subsequently, stimulation of antitumor immune-response [76], this cytokine was increased in the M1-stimulated group, suggesting a more anti-tumor profile, along with MIP, MCP-3 and IL-8 (known to act on recruitment and activation of immune cells, including macrophages), M-CSF (involved in the differentiation, survival, and activation of macrophages) [77]. IL-1β is a pro-inflammatory cytokine that, was, as expected increased in the M1 stimulated group. This cytokine can influence the inflammatory response and potentially impact tumor progression and invasion, with a dual anti-tumor/pro-tumor role [78]. Yet, it is also clear from our data that many other molecules demonstrated to impact favorably OS progression were also increased in the M1 profile, namely TGF-α [79], IL-6 [78], suggesting that the immunomodulation of the TME is a complex process and ultimately requires other combined weapons, targeting not only immune cells but also other cells of the TME. Future studies will be required to evaluate the impact of this shift on tumor progression and inhibition of an invasive behavior. Also, it is important to note that the specific roles of these molecules in OS can vary based on the stage of the disease, the TME, and the interplay between different signaling pathways, therefore, a deeper understanding of these roles will be crucial for developing targeted therapies and improving treatment strategies. The GO analysis revealed an increase in biological processes associated with B cell proliferation, activation, and immunoglobulin production. This finding is consistent with the observed shift in the MCTS TME, towards more a pro-inflammatory, anti-tumoral activity (M1-like). Elevated levels of IFN-γ and IL-12 by TAMs have been described to act on B cell activation [80]. Notably, IFN-γ can enhance the antibody-producing capabilities of B cells [81]. Furthermore, M1-polarized macrophages have the ability to present antigens to B cells, thereby amplifying B cell activation and initiating the production of antibodies against cancer cells. Overall, the crosstalk between M1 macrophages and B cells is likely to impact the regulatory functions of B cells, influencing their ability to modulate the immune response. This intricate interaction has broader implications, extending to other immune cells, such as natural killer (NK) cells, through

antibody-dependent cellular cytotoxicity. In this process, antibodies attach to cancer cells, and immune cells, equipped with Fc receptors, recognize and bind to the Fc portion of the antibodies, leading to the destruction of cancer cells [82]. This modulation can impact the balance between anti-tumor immunity and potential immunosuppressive mechanisms within the TME. Altogether, this finding points to the TME, namely through the modulation of immune and stromal cells, as a potential targets for the development of novel therapies. Aiming at exploring this opportunity, an immunomodulatory/immunostimulatory molecule, MDP, was selected for encapsulation in a polymeric nanosystem to validate the drug screening potential of our model using an approved OS TME targeted therapy. Although MDP is currently available as the only immunomodulatory therapy for OS, several MDP analogues have shown motivating results [83]. In our study, we observed a dose-dependent cytotoxicity in mono culture spheroids, but this profile was roughly lost as the immune and the stromal populations are included (Fig. 4S), supporting described role of the TME and particularly of the stromal and immune cells drug resistance mechanisms [84]. When looking at the secretome changes of triple culture spheroids, the reversion towards an M1-like phenotype of the secretome could be seen for the two highest concentrations of MDP-loaded NPs, presenting a contrasting profile of soluble factors when compared with the M2 control. Free MDP, at the same concentrations, exhibited a limited capacity at reverting the pro-tumoral profile of the OS TME, highlighting the advantages of using nanocarriers to improve the efficacy of drugs/molecules when encapsulated. By demonstrating the TME's immunomodulation responsiveness of our model also using an immunomodulatory nanosystems, we have further shown the potential of multicellular and heterotypic 3D models in novel therapies screening in the early drug development stages.

This study pioneers a fully humanized 3D OS model that closely replicates the native tumor environment. This model offers significant opportunities to deepen our understanding of OS pathophysiology and, importantly, to drive the development of novel therapeutic approaches that can be screened in a biologically relevant model. This represents a substantial advance over existing OS models, which primarily rely on tumor cells alone [85] or, more recently, on combinations with stromal cells and ECM-like matrices [86], often overlooking the critical role of immune cells in tumor development, behavior and response to treatment. By providing a fully humanized *in vitro* 3D system, our MCTS bridges the gap between traditional 2D cell cultures and animal models in OS research, with high translational by minimizing species-specific discrepancies in drug responses. Additionally, our model demonstrates dynamic responsiveness of the TME, including shifts in macrophage polarization and in the secretome — a feature that hasn't been described on other OS models *in vitro*, and that can be further explored into innovative therapeutic interventions, particularly those targeting tumor-immune interactions. Remarkably, we have successfully established an *in vitro* tumor with a pro-tumor phenotype that reflects the aggressive nature characteristic of pediatric OS. The model's ease of establishment, metabolic activity for up to 10 days, and high-throughput compatibility presents significant advantages over other models, enhancing its applicability but also as a valuable preclinical screening tool in the drug development pipeline. Our scaffold-free model with the capacity of producing their own ECM, offers multiple advantages, such as the replication of adhesion ligand complexity, ease of remodeling, and cytokine interaction while offering TME tunability and reduced batch-to-batch variability [87]. Notably, the principles and techniques used to develop this 3D *in vitro* model of OS can be adapted to other bone cancers, such as Ewing sarcoma or chondrosarcoma, by incorporating specific cell types from each tumor to create relevant TMEs. This is particularly pertinent given the growing interest in immunotherapies and macrophage targeting approaches for these bone cancers [88,89]. Additionally, as personalized medicine advances, this model could be set using patient-derived cells, providing a versatile platform to study patient-specific responses to multimodal therapies for a range of bone tumors.

Consent for publication

All the authors are consent for publication.

Ethics approval

Monocytes used in this study were isolated from buffy coats of healthy blood donors kindly provided by the immunohemotherapy department of Centro Hospitalar Universitário São João (CHUSJ), Porto, Portugal, under the ethical agreement number: 90/19. Donors provided written consent for their blood to be used for research purposes. This study was approved by CECRI (Commission for Ethics and Responsible Conduct in Research of i3S), Appraisal N21/CECRI/2022.

Funding

This research supported had the support of Liga Portuguesa Contra o Cancro (LPCC) - Bolsa em Sarcomas Pediatricos Nonô (NN 2023-25 CP Fellowship) and Fundação para a Ciência e Tecnologia trough RESTART funded MICKEY project (2023.00095.RESTART). CLP (UIDP/04293/2020) and FCT (2021.01773.CEECIND) are supported by FCT, JV is a Marie Curie Postdoctoral Fellow (GA: 101130766).

Author contributions

S.C.: Conducted the research and investigation process, specifically performing the experiments and the respective data/evidence collection, Writing (review and editing); J.R.: Conducted the research and investigation process, Writing (review and editing); C.V. Conducted the research and investigation process, Writing (review and editing); S.D.: Conducted the research and investigation process; J.V.: Conducted the research and investigation process; F.C.: Conceptualization, Data discussion, Writing (review and editing); B.S.: Resources, Writing (review and editing); C.L.P.: Conceptualization, Funding Acquisition, Resources, Writing (original draft, review and editing).

CRediT authorship contribution statement

João Rodrigues: Writing – original draft, Methodology, Investigation, Data curation. **Carolina Vieira:** Writing – original draft, Methodology, Formal analysis, Data curation. **Sofia Dias:** Writing – original draft, Methodology, Formal analysis, Data curation. **Juliana Viegas:** Writing – review & editing, Supervision, Methodology, Investigation, Formal analysis, Data curation. **Flávia Castro:** Writing – review & editing, Methodology, Data curation, Conceptualization. **Bruno Sarmento:** Writing – review & editing, Supervision, Resources, Project administration. **Catarina Leite Pereira:** Writing – review & editing, Writing – original draft, Supervision, Resources, Project administration, Methodology, Investigation, Funding acquisition, Data curation, Conceptualization.

Declaration of competing interest

The authors declare that they have no competing interests.

Data availability

All data generated or analyzed during this study are included in this published article and its supplementary information files.

Acknowledgements

The authors express gratitude to Dr. André Maia and Dr. Rita Reis from the BioSciences Screening Platform at i3S for their technical

support in optimizing 3D dimensional imaging acquisition. Special thanks to the Bioinformatics platform at i3S, especially Dr. Bruno Cavadas (CEECINST/00123/2021/CP1772/CT0001), for the multiplex data analysis/plotting. Additional acknowledgments go to the Histology and Electron Microscopy platform at i3S, specifically to Rui Fernandes, Claudia Machado, and Sofia Pacheco from the Histology Unit, and Dr. Emilia Cardoso from the Translational Cytometry Platform at i3S for her support in data acquisition.

Appendix A. Supplementary data

Supplementary data to this article can be found online at https://doi.org/10.1016/j.jconrel.2024.10.068.

References

[1] L. Mirabello, R.J. Troisi, S.A. Savage, International osteosarcoma incidence patterns in children and adolescents, middle ages and elderly persons, Int. J. Cancer 125 (2009) 229–234, https://doi.org/10.1002/ijc.24320.
[2] A.J. Saraf, J.M. Fenger, R.D. Roberts, Osteosarcoma: accelerating progress makes for a hopeful future, Front. Oncol. 8 (2018) 4, https://doi.org/10.3389/fonc.2018.00004.
[3] A.M. Czarnecka, K. Synoradzki, W. Firlej, E. Bartnik, P. Sobczuk, M. Fiedorowicz, P. Grieb, P. Rutkowski, Molecular biology of osteosarcoma, Cancers (Basel) 12 (2020), https://doi.org/10.3390/cancers12082130.
[4] J. Rodrigues, B. Sarmento, C.L. Pereira, Osteosarcoma tumor microenvironment: the key for the successful development of biologically relevant 3D in vitro models, In vitro models 1 (2022) 5–27, https://doi.org/10.1007/s44164-022-00008-x.
[5] C.F. Monteiro, S.C. Santos, C.A. Custódio, J.F. Mano, Human platelet lysates-based hydrogels: a novel personalized 3D platform for spheroid invasion assessment, Adv. Sci. 7 (2020) 1902398, https://doi.org/10.1002/advs.201902398.
[6] A. De Luca, L. Raimondi, F. Salamanna, V. Carina, V. Costa, D. Bellavia, R. Alessandro, M. Fini, G. Giavaresi, Relevance of 3d culture systems to study osteosarcoma environment, J. Exp. Clin. Cancer Res. 37 (2018) 2, https://doi.org/10.1186/s13046-017-0663-5.
[7] P. Kunz, A. Schenker, H. Sähr, B. Lehner, J. Fellenberg, Optimization of the chicken chorioallantoic membrane assay as reliable in vivo model for the analysis of osteosarcoma, PLoS One 14 (2019) e0215312, https://doi.org/10.1371/journal.pone.0215312.
[8] M.M. Lizardo, P.H. Sorensen, Practical considerations in studying metastatic lung colonization in osteosarcoma using the pulmonary metastasis assay, J. Vis. Exp. (2018), https://doi.org/10.3791/56332.
[9] E.T.H. Ek, C.R. Dass, P.F.M. Choong, Commonly used mouse models of osteosarcoma, Crit. Rev. Oncol. Hematol. 60 (2006) 1–8, https://doi.org/10.1016/j.critrevonc.2006.03.006.
[10] Z. Duan, Y. Luo, Targeting macrophages in cancer immunotherapy, Signal Transduct. Target. Ther. 6 (2021) 127, https://doi.org/10.1038/s41392-021-00506-6.
[11] E.P. Buddingh, M.L. Kuijjer, R.A. Duim, H. Burger, K. Agelopoulos, O. Myklebost, M. Serra, F. Mertens, P.C. Hogendoorn, A.C. Lankester, A.M. Cleton-Jansen, Tumor-infiltrating macrophages are associated with metastasis suppression in high-grade osteosarcoma: a rationale for treatment with macrophage activating agents, Clin. Cancer Res. 17 (2011) 2110–2119, https://doi.org/10.1158/1078-0432.CCR-10-2047.
[12] Y. Han, W. Guo, T. Ren, Y. Huang, S. Wang, K. Liu, B. Zheng, K. Yang, H. Zhang, X. Liang, Tumor-associated macrophages promote lung metastasis and induce epithelial-mesenchymal transition in osteosarcoma by activating the COX-2/STAT3 axis, Cancer Lett. 440-441 (2019) 116–125, https://doi.org/10.1016/j.canlet.2018.10.011.
[13] M.F. Heymann, F. Lezot, D. Heymann, The contribution of immune infiltrates and the local microenvironment in the pathogenesis of osteosarcoma, Cell. Immunol. 343 (2019) 103711, https://doi.org/10.1016/j.cellimm.2017.10.011.
[14] C. Dumars, J.M. Ngyuen, A. Gaultier, R. Lanel, N. Corradini, F. Gouin, D. Heymann, M.F. Heymann, Dysregulation of macrophage polarization is associated with the metastatic process in osteosarcoma, Oncotarget 7 (2016) 78343–78354, https://doi.org/10.18632/oncotarget.13055.
[15] P. Dhupkar, N. Gordon, J. Stewart, E.S. Kleinerman, Anti-PD-1 therapy redirects macrophages from an M2 to an M1 phenotype inducing regression of OS lung metastases, Cancer Med. 7 (2018) 2654–2664, https://doi.org/10.1002/cam4.1518.
[16] D. Ryan, B.T. Paul, J. Koziol, W.M. ElShamy, The pro- and anti-tumor roles of mesenchymal stem cells toward BRCA1-IRIS-overexpressing TNBC cells, Breast Cancer Res. 21 (2019) 53, https://doi.org/10.1186/s13058-019-1131-2.
[17] U. Blache, E.R. Horton, T. Xia, E.M. Schoof, L.H. Blicher, A. Schönenberger, J. G. Snedeker, I. Martin, J.T. Erler, M. Ehrbar, Mesenchymal stromal cell activation by breast cancer secretomes in bioengineered 3D microenvironments, Life Sci. Alliance 2 (2019), https://doi.org/10.26508/lsa.201900304.
[18] Y. Shi, L. Du, L. Lin, Y. Wang, Tumour-associated mesenchymal stem/stromal cells: emerging therapeutic targets, Nat. Rev. Drug Discov. 16 (2017) 35–52, https://doi.org/10.1038/nrd.2016.193.
[19] P.M. Anderson, P. Meyers, E. Kleinerman, K. Venkatakrishnan, D.P. Hughes, C. Herzog, W. Huh, R. Sutphin, Y.M. Vyas, V. Shen, et al., Mifamurtide in metastatic and recurrent osteosarcoma: a patient access study with pharmacokinetic, pharmacodynamic, and safety assessments, Pediatr. Blood Cancer 61 (2014) 238–244, https://doi.org/10.1002/pbc.24686.
[20] N. Nastasi, A. Pasha, G. Bruno, A. Subbiani, L. Pietrovito, A. Leo, L. Scala, L. de Simone, G. Casazza, F. Lunardi, et al., Blockade of IL-10 signaling ensures mifamurtide efficacy in metastatic osteosarcoma, Cancers (Basel) 15 (2023), https://doi.org/10.3390/cancers15194744.
[21] F. Hirschhaeuser, H. Menne, C. Dittfeld, J. West, W. Mueller-Klieser, L.A. Kunz-Schughart, Multicellular tumor spheroids: an underestimated tool is catching up again, J. Biotechnol. 148 (2010) 3–15, https://doi.org/10.1016/j.jbiotec.2010.01.012.
[22] A.P. Napolitano, D.M. Dean, A.J. Man, J. Youssef, D.N. Ho, A.P. Rago, M.P. Lech, J. R. Morgan, Scaffold-free three-dimensional cell culture utilizing micromolded nonadhesive hydrogels, BioTechniques 43 (2007) 494–500, https://doi.org/10.2144/000112591.
[23] J. Carlsson, J. Yuhas, Liquid-overlay culture of cellular spheroids, in: Spheroids in Cancer Research: Methods and Perspectives, 1984, pp. 1–23.
[24] Q. Huang, X. Liang, T. Ren, Y. Huang, H. Zhang, Y. Yu, C. Chen, W. Wang, J. Niu, J. Lou, W. Guo, The role of tumor-associated macrophages in osteosarcoma progression – therapeutic implications, Cell. Oncol. 44 (2021) 525–539, https://doi.org/10.1007/s13402-021-00598-w.
[25] X. Chang, Z. Ma, G. Zhu, Y. Lu, J. Yang, New perspective into mesenchymal stem cells: molecular mechanisms regulating osteosarcoma, J. Bone Oncol. 29 (2021) 100372, https://doi.org/10.1016/j.jbo.2021.100372.
[26] A.B. Mohseny, I. Machado, Y. Cai, K.L. Schaefer, M. Serra, P.C. Hogendoorn, A. Llombart-Bosch, A.M. Cleton-Jansen, Functional characterization of osteosarcoma cell lines provides representative models to study the human disease, Lab. Investig. 91 (2011) 1195–1205, https://doi.org/10.1038/labinvest.2011.72.
[27] Y. Petrenko, I. Vackova, K. Kekulova, M. Chudickova, Z. Koci, K. Turnovcova, H. Kupcova Skalnikova, P. Vodicka, S. Kubinova, A comparative analysis of multipotent mesenchymal stromal cells derived from different sources, with a focus on neuroregenerative potential, Sci. Rep. 10 (2020) 4290, https://doi.org/10.1038/s41598-020-61167-z.
[28] F.E. Freeman, R. Burdis, O.R. Mahon, D.J. Kelly, N. Artzi, A spheroid model of early and late-stage osteosarcoma mimicking the divergent relationship between tumor elimination and bone regeneration, Adv. Healthc. Mater. 11 (2022) e2101296, https://doi.org/10.1002/adhm.202101296.
[29] C.F. Monteiro, C.A. Custódio, J.F. Mano, Three-dimensional osteosarcoma models for advancing drug discovery and development, Adv. Ther. 2 (2019) 1800108, https://doi.org/10.1002/adtp.201800108.
[30] I. Corre, F. Verrecchia, V. Crenn, F. Redini, V. Trichet, The osteosarcoma microenvironment: a complex but targetable ecosystem, Cells 9 (2020), https://doi.org/10.3390/cells9040976.
[31] B. Erdogan, M. Ao, L.M. White, A.L. Means, B.M. Brewer, L. Yang, M. K. Washington, C. Shi, O.E. Franco, A.M. Weaver, et al., Cancer-associated fibroblasts promote directional cancer cell migration by aligning fibronectin, J. Cell Biol. 216 (2017) 3799–3816, https://doi.org/10.1083/jcb.201704053.
[32] J. Wang, D. Li, H. Cang, B. Guo, Crosstalk between cancer and immune cells: role of tumor-associated macrophages in the tumor microenvironment, Cancer Med. 8 (2019) 4709–4721, https://doi.org/10.1002/cam4.2327.
[33] X.J. Shao, S.F. Xiang, Y.Q. Chen, N. Zhang, J. Cao, H. Zhu, B. Yang, Q. Zhou, M. D. Ying, Q.J. He, Inhibition of M2-like macrophages by all-trans retinoic acid prevents cancer initiation and stemness in osteosarcoma cells, Acta Pharmacol. Sin. 40 (2019) 1343–1350, https://doi.org/10.1038/s41401-019-0262-4.
[34] Q. Han, H. Shi, F. Liu, CD163(+) M2-type tumor-associated macrophage support the suppression of tumor-infiltrating T cells in osteosarcoma, Int. Immunopharmacol. 34 (2016) 101–106, https://doi.org/10.1016/j.intimp.2016.01.023.
[35] Q. Xiao, X. Zhang, Y. Wu, Y. Yang, Inhibition of macrophage polarization prohibits growth of human osteosarcoma, Tumour Biol. 35 (2014) 7611–7616, https://doi.org/10.1007/s13277-014-2005-y.
[36] P. Zheng, W. Li, Crosstalk between mesenchymal stromal cells and tumor-associated macrophages in gastric cancer, Front. Oncol. 10 (2020) 571516, https://doi.org/10.3389/fonc.2020.571516.
[37] W. Li, X. Zhang, F. Wu, Y. Zhou, Z. Bao, H. Li, P. Zheng, S. Zhao, Gastric cancer-derived mesenchymal stromal cells trigger M2 macrophage polarization that promotes metastasis and EMT in gastric cancer, Cell Death Dis. 10 (2019) 918, https://doi.org/10.1038/s41419-019-2131-y.
[38] M. Oshi, Y. Tokumaru, M. Asaoka, L. Yan, V. Satyananda, R. Matsuyama, N. Matsuhashi, M. Futamura, T. Ishikawa, K. Yoshida, et al., M1 macrophage and M1/M2 ratio defined by transcriptomic signatures resemble only part of their conventional clinical characteristics in breast cancer, Sci. Rep. 10 (2020) 16554, https://doi.org/10.1038/s41598-020-73624-w.
[39] F. Paradiso, S. Serpelloni, L.W. Francis, F. Taraballi, Mechanical studies of the third dimension in cancer: from 2D to 3D model, Int. J. Mol. Sci. 22 (2021), https://doi.org/10.3390/ijms221810098.
[40] R. Elenjord, J.B. Allen, H.T. Johansen, H. Kildalsen, G. Svineng, G.M. Maelandsmo, T. Loennechen, J.-O. Winberg, Collagen I regulates matrix metalloproteinase-2 activation in osteosarcoma cells independent of S100A4, FEBS J. 276 (2009) 5275–5286, https://doi.org/10.1111/j.1742-4658.2009.07223.x.
[41] C. Gebhard, C. Gabriel, I. Walter, Morphological and immunohistochemical characterization of canine osteosarcoma spheroid cell cultures, Anat. Histol. Embryol. 45 (2016) 219–230, https://doi.org/10.1111/ahe.12190.

[42] J.H. Nie, T. Yang, H. Li, H.S. Ye, G.Q. Zhong, T.T. Li, C. Zhang, W.H. Huang, J. Xiao, Z. Li, et al., Identification of GPC3 mutation and upregulation in a multidrug resistant osteosarcoma and its spheroids as therapeutic target, J. Bone Oncol. 30 (2021) 100391, https://doi.org/10.1016/j.jbo.2021.100391.
[43] M.V. Monteiro, V.M. Gaspar, L.P. Ferreira, J.F. Mano, Hydrogel 3D in vitro tumor models for screening cell aggregation mediated drug response, Biomater. Sci. 8 (2020) 1855–1864, https://doi.org/10.1039/c9bm02075f.
[44] M. Rimann, S. Laternser, A. Gvozdenovic, R. Muff, B. Fuchs, J.M. Kelm, U. Graf-Hausner, An in vitro osteosarcoma 3D microtissue model for drug development, J. Biotechnol. 189 (2014) 129–135, https://doi.org/10.1016/j.jbiotec.2014.09.005.
[45] B.M. Leung, S.C. Lesher-Perez, T. Matsuoka, C. Moraes, S. Takayama, Media additives to promote spheroid circularity and compactness in hanging drop platform, Biomater. Sci. 3 (2015) 336–344.
[46] J.A. Zimmermann, T.C. McDevitt, Pre-conditioning mesenchymal stromal cell spheroids for immunomodulatory paracrine factor secretion, Cytotherapy 16 (2014) 331–345, https://doi.org/10.1016/j.jcyt.2013.09.004.
[47] G.A. Hamilton, C. Westmoreland, E. George, Effects of medium composition on the morphology and function of rat hepatocytes cultured as spheroids and monolayers, In Vitro Cell. Dev. Biol. Anim. 37 (2001) 656–667.
[48] F. Keller, R. Rudolf, M. Hafner, Towards optimized breast cancer 3D spheroid mono- and co-culture models for pharmacological research and screening, J. Cell. Biotechnol. 5 (2019) 89–101, https://doi.org/10.3233/jcb-199001.
[49] P. Indovina, G. Rainaldi, M.T. Santini, Hypoxia increases adhesion and spreading of MG-63 three-dimensional tumor spheroids, Anticancer Res. 28 (2008) 1013–1022.
[50] F. Cersosimo, S. Lonardi, G. Bernardini, B. Telfer, G.E. Mandelli, A. Santucci, W. Vermi, E. Giurisato, Tumor-associated macrophages in osteosarcoma: from mechanisms to therapy, Int. J. Mol. Sci. 21 (2020), https://doi.org/10.3390/ijms21155207.
[51] T. Zhu, J. Han, L. Yang, Z. Cai, W. Sun, Y. Hua, J. Xu, Immune microenvironment in osteosarcoma: components, therapeutic strategies and clinical applications, Front. Immunol. 13 (2022) 907550, https://doi.org/10.3389/fimmu.2022.907550.
[52] A.J. Mutsaers, C.R. Walkley, Cells of origin in osteosarcoma: mesenchymal stem cells or osteoblast committed cells? Bone 62 (2014) 56–63, https://doi.org/10.1016/j.bone.2014.02.003.
[53] V.K. Sarhadi, R. Daddali, R. Seppanen-Kaijansinkko, Mesenchymal stem cells and extracellular vesicles in osteosarcoma pathogenesis and therapy, Int. J. Mol. Sci. 22 (2021), https://doi.org/10.3390/ijms222011035.
[54] W.T. Xu, Z.Y. Bian, Q.M. Fan, G. Li, T.T. Tang, Human mesenchymal stem cells (hMSCs) target osteosarcoma and promote its growth and pulmonary metastasis, Cancer Lett. 281 (2009) 32–41, https://doi.org/10.1016/j.canlet.2009.02.022.
[55] H. Zhang, J. Wang, T. Ren, Y. Huang, X. Liang, Y. Yu, W. Wang, J. Niu, W. Guo, Bone marrow mesenchymal stem cell-derived exosomal miR-206 inhibits osteosarcoma progression by targeting TRA2B, Cancer Lett. 490 (2020) 54–65, https://doi.org/10.1016/j.canlet.2020.07.008.
[56] J.H. Ylostalo, T.J. Bartosh, K. Coble, D.J. Prockop, Human mesenchymal stem/stromal cells cultured as spheroids are self-activated to produce prostaglandin E2 that directs stimulated macrophages into an anti-inflammatory phenotype, Stem Cells 30 (2012) 2283–2296, https://doi.org/10.1002/stem.1191.
[57] M. Cortini, A. Massa, S. Avnet, G. Bonuccelli, N. Baldini, Tumor-activated mesenchymal stromal cells promote osteosarcoma stemness and migratory potential via IL-6 secretion, PLoS One 11 (2016) e0166500, https://doi.org/10.1371/journal.pone.0166500.
[58] N.L. Tran, I.K. Lee, H. Kim, K. Lee, S.-H. Kim, S.J. Oh, Facile construction of tumour spheroids with induced M2 macrophage polarization for anticancer drug screening, Biomed. Mater. 17 (2022) 065015.
[59] J.K. Mouw, G. Ou, V.M. Weaver, Extracellular matrix assembly: a multiscale deconstruction, Nat. Rev. Mol. Cell Biol. 15 (2014) 771–785, https://doi.org/10.1038/nrm3902.
[60] T. Wiklund, C. Blomqvist, L. Risteli, J. Risteli, E. Karaharju, I. Elomaa, Type I and type III collagen metabolites in adult osteosarcoma patients, Br. J. Cancer 73 (1996) 106–109, https://doi.org/10.1038/bjc.1996.19.
[61] K. Shi, S.-L. Wang, B. Shen, F.-Q. Yu, D.-F. Weng, J.-H. Lin, Clinicopathological and prognostic values of fibronectin and integrin αvβ3 expression in primary osteosarcoma, World J. Surg. Oncol. 17 (2019), https://doi.org/10.1186/s12957-019-1566-z.
[62] M. Cortini, F. Macchi, F. Reggiani, E. Vitale, M.V. Lipreri, F. Perut, A. Ciarrocchi, N. Baldini, S. Avnet, Endogenous extracellular matrix regulates the response of osteosarcoma 3D spheroids to doxorubicin, Cancers 15 (2023) 1221, https://doi.org/10.3390/cancers15041221.
[63] A.L.S. Cruz, E.D.A. Barreto, N.P.B. Fazolini, J.P.B. Viola, P.T. Bozza, Lipid droplets: platforms with multiple functions in cancer hallmarks, Cell Death Dis. 11 (2020), https://doi.org/10.1038/s41419-020-2297-3.
[64] P. Schwartsburd, Lipid droplets: could they be involved in cancer growth and cancer–microenvironment communications? Cancer Commun. 42 (2022) 83–87, https://doi.org/10.1002/cac2.12257.
[65] H. Wu, Y. Han, Y. Rodriguez Sillke, H. Deng, S. Siddiqui, C. Treese, F. Schmidt, M. Friedrich, J. Keye, J. Wan, et al., Lipid droplet-dependent fatty acid metabolism controls the immune suppressive phenotype of tumor-associated macrophages, EMBO Mol. Med. 11 (2019) e10698, https://doi.org/10.15252/emmm.201910698.
[66] N. Leitner, J. Hlavatý, R. Ertl, S. Gabner, A. Fuchs-Baumgartinger, I. Walter, Lipid droplets and perilipins in canine osteosarcoma. Investigations on tumor tissue, 2D and 3D cell culture models, Vet. Res. Commun. 46 (2022) 1175–1193, https://doi.org/10.1007/s11259-022-09975-8.
[67] M. Cortini, A. Armirotti, M. Columbaro, D.L. Longo, G. Di Pompo, E. Cannas, A. Maresca, C. Errani, A. Longhi, A. Righi, et al., Exploring metabolic adaptations to the acidic microenvironment of osteosarcoma cells unveils sphingosine 1-phosphate as a valuable therapeutic target, Cancers 13 (2021) 311, https://doi.org/10.3390/cancers13020311.
[68] Y. Jin, Y. Tan, J. Wu, Z. Ren, Lipid droplets: a cellular organelle vital in cancer cells, Cell Death Discov. 9 (2023), https://doi.org/10.1038/s41420-023-01493-z.
[69] Y. Tanaka, M. Nishikawa, Y. Mizukami, K. Kusamori, Y. Ogino, S. Nishimura, K. Shimizu, S. Konishi, Y. Takahashi, Y. Takakura, Control of polarization and tumoricidal activity of macrophages by multicellular spheroid formation, J. Control. Release 270 (2018) 177–183, https://doi.org/10.1016/j.jconrel.2017.12.006.
[70] H. Tang, Y. Zhang, J.A. Jansen, J.J.J.P. van den Beucken, Effect of monocytes/macrophages on the osteogenic differentiation of adipose-derived mesenchymal stromal cells in 3D co-culture spheroids, Tissue Cell 49 (2017) 461–469, https://doi.org/10.1016/j.tice.2017.06.002.
[71] I. Bhavsar, C.S. Miller, M. Al-Sabbagh, Macrophage Inflammatory Protein-1 Alpha (MIP-1 alpha)/CCL3: As a Biomarker, Gen. Methods Biomark. Res. Applic. (2015 Jun 1) 223–249, https://doi.org/10.1007/978-94-007-7696-8_27.
[72] S.W. Wang, H.H. Wu, S.C. Liu, P.C. Wang, W.C. Ou, W.Y. Chou, Y.S. Shen, C. H. Tang, CCL5 and CCR5 interaction promotes cell motility in human osteosarcoma, PLoS One 7 (2012) e35101, https://doi.org/10.1371/journal.pone.0035101.
[73] S.W. Wang, S.C. Liu, H.L. Sun, T.Y. Huang, C.H. Chan, C.Y. Yang, H.I. Yeh, Y. L. Huang, W.Y. Chou, Y.M. Lin, C.H. Tang, CCL5/CCR5 axis induces vascular endothelial growth factor-mediated tumor angiogenesis in human osteosarcoma microenvironment, Carcinogenesis 36 (2015) 104–114, https://doi.org/10.1093/carcin/bgu218.
[74] K. Sun, C. Gong, H. Peng, H. Fang, J. Zhou, J. Li, S. Chen, H. Zheng, High CCL5 expression is associated with osteosarcoma metastasis and poor prognosis of patients with osteosarcoma, Mol. Med. Rep. 16 (2017) 6953–6957, https://doi.org/10.3892/mmr.2017.7458.
[75] D. Aldinucci, C. Borghese, N. Casagrande, The CCL5/CCR5 axis in cancer progression, Cancers (Basel) 12 (2020), https://doi.org/10.3390/cancers12071765.
[76] D. Jorgovanovic, M. Song, L. Wang, Y. Zhang, Roles of IFN-γ in tumor progression and regression: a review, Biomark. Res. 8 (2020) 49, https://doi.org/10.1186/s40364-020-00228-x.
[77] H. Li, M. Wu, X. Zhao, Role of chemokine systems in cancer and inflammatory diseases, MedComm 3 (2022) e147, https://doi.org/10.1002/mco2.147.
[78] K.J. Baker, A. Houston, E. Brint, IL-1 family members in cancer; two sides to every story, Front. Immunol. 10 (2019) 1197, https://doi.org/10.3389/fimmu.2019.01197.
[79] C.H. Hou, F.L. Lin, K.B. Tong, S.M. Hou, J.F. Liu, Transforming growth factor alpha promotes osteosarcoma metastasis by ICAM-1 and PI3K/Akt signaling pathway, Biochem. Pharmacol. 89 (2014) 453–463, https://doi.org/10.1016/j.bcp.2014.03.010.
[80] X. Ma, TNF-α and IL-12:a balancing act in macrophage functioning, Microbes Infect. 3 (2001) 121–129, https://doi.org/10.1016/S1286-4579(00)01359-9.
[81] E. Alspach, D.M. Lussier, R.D. Schreiber, Interferon γ and its important roles in promoting and inhibiting spontaneous and therapeutic cancer immunity, Cold Spring Harb. Perspect. Biol. 11 (2019), https://doi.org/10.1101/cshperspect.a028480.
[82] G.S. Kinker, G.A.F. Vitiello, W.A.S. Ferreira, A.S. Chaves, V.C. Cordeiro de Lima, Medina, T.d.S., B cell orchestration of anti-tumor immune responses: a matter of cell localization and communication, Front. Cell Dev. Biol. 9 (2021), https://doi.org/10.3389/fcell.2021.678127.
[83] E. Iwicka, J. Hajtuch, K. Dzierzbicka, I. Inkielewicz-Stepniak, Muramyl dipeptide-based analogs as potential anticancer compounds: strategies to improve selectivity, biocompatibility, and efficiency, Front. Oncol. 12 (2022) 970967, https://doi.org/10.3389/fonc.2022.970967.
[84] Y. Ni, X. Zhou, J. Yang, H. Shi, H. Li, X. Zhao, X. Ma, The role of tumor-stroma interactions in drug resistance within tumor microenvironment, Front. Cell Dev. Biol. 9 (2021) 637675, https://doi.org/10.3389/fcell.2021.637675.
[85] J. Munoz-Garcia, C. Jubelin, A. Loussouarn, M. Goumard, L. Griscom, A. Renodon-Cornière, M.-F. Heymann, D. Heymann, In vitro three-dimensional cell cultures for bone sarcomas, J. Bone Oncol. 30 (2021) 100379, https://doi.org/10.1016/j.jbo.2021.100379.
[86] C.F. Monteiro, C.A. Custódio, J.F. Mano, Bioengineering a humanized 3D tri-culture osteosarcoma model to assess tumor invasiveness and therapy response, Acta Biomater. 134 (2021) 204–214, https://doi.org/10.1016/j.actbio.2021.07.034.
[87] T. Gonzalez-Fernandez, A.J. Tenorio, A.M. Saiz Jr., J.K. Leach, Engineered cell-secreted extracellular matrix modulates cell spheroid mechanosensing and amplifies their response to inductive cues for the formation of mineralized tissues, Adv. Healthc. Mater. 11 (2022) 2102337, https://doi.org/10.1002/adhm.202102337.
[88] R. Iseulys, G.B. Anne, B. Corinne, D.B.P. Gonzague, K. Marie, B. Jean-Yves, D. Aurélie, The immune landscape of chondrosarcoma reveals an immunosuppressive environment in the dedifferentiated subtypes and exposes CSFR1+ macrophages as a promising therapeutic target, J. Bone Oncol. 20 (2020) 100271, https://doi.org/10.1016/j.jbo.2019.100271.
[89] W. Luo, H. Hoang, K.E. Miller, H. Zhu, S. Xu, X. Mo, E.A.R. Garfinkle, H. Costello, S. Wijeratne, W. Chemnitz, et al., Combinatorial macrophage induced innate

immunotherapy against Ewing sarcoma: turning “two keys” simultaneously, J. Exp. Clin. Cancer Res. 43 (2024) 193, https://doi.org/10.1186/s13046-024-03093-w.